

**RESEARCH ARTICLE**

10.1029/2018JE005663

**Special Section:**

Planetary Mapping: Methods,  
Tools for Scientific Analysis and  
Exploration

This article is a companion to Séjourné  
et al. (2018), <https://doi.org/10.1029/2018JE005665>; Orgel et al. (2018),  
<https://doi.org/10.1029/2018JE005664>.

**Key Points:**

- We mapped the latitude-dependent mantle (LDM) almost ubiquitously from 35°N to 78°N; this correlates with predicted ground ice stability
- Degradational features into the LDM (pits, scallops, and polygons) suggest ground ice and volatile loss between 35 and 70°N in Arcadia
- The LDM has air fall origin; however, air fall, fluvial, and underlying processes are equally dominant in shaping the northern plains of Mars

**Correspondence to:**

J. D. Ramsdale,  
[jason.ramsdale@nmggroup.com](mailto:jason.ramsdale@nmggroup.com)

**Citation:**

Ramsdale, J. D., Balme, M. R., Gallagher, C., Conway, S. J., Smith, I. B., Hauber, E., et al. (2019). Grid mapping the northern plains of Mars: Geomorphological, radar, and water-equivalent hydrogen results from Arcadia Planitia. *Journal of Geophysical Research: Planets*, 124, 504–527. <https://doi.org/10.1029/2018JE005663>






Received 6 MAY 2018

Accepted 25 JUL 2018

Accepted article online 13 SEP 2018

Published online 22 FEB 2019

# Grid Mapping the Northern Plains of Mars: Geomorphological, Radar, and Water-Equivalent Hydrogen Results From Arcadia Planitia

Jason D. Ramsdale<sup>1</sup> , Matthew R. Balme<sup>1</sup> , Colman Gallagher<sup>2,3</sup> , Susan J. Conway<sup>1,4</sup> , Isaac B. Smith<sup>5</sup> , Ernst Hauber<sup>6</sup>, Csilla Orgel<sup>6,7</sup> , Antoine Séjourné<sup>8</sup> , Francois Costard<sup>8</sup> , Vince R. Eke<sup>9</sup>, Stephan A. van Gasselt<sup>10</sup> , Andreas Johnsson<sup>11</sup>, Akos Kereszturi<sup>12</sup>, Anna Losiak<sup>13,14</sup>, Richard J. Massey<sup>9</sup>, Thomas Platz<sup>15,16</sup> , Dennis Reiss<sup>17</sup>, James A. Skinner<sup>18</sup>, Zuzanna M. Swirad<sup>19</sup> , Luis F. A. Teodoro<sup>20</sup>, and Jack T. Wilson<sup>1,21</sup> 

<sup>1</sup>Department of Physical Sciences, The Open University, Milton Keynes, UK, <sup>2</sup>UCD School of Geography, University College Dublin, Dublin, Ireland, <sup>3</sup>UCD Earth Institute, University College Dublin, Dublin, Ireland, <sup>4</sup>Laboratoire de Planétologie et Géodynamique–UMR CNRS 6112, Nantes, France, <sup>5</sup>Institute for Geophysics, J.J. Pickle Research Campus, University of Texas at Austin, Austin, TX, USA, <sup>6</sup>DLR-Institut für Planetenforschung, Berlin, Germany, <sup>7</sup>Institute of Geological Sciences Planetary Sciences and Remote Sensing, Freie Universität Berlin, Berlin, Germany, <sup>8</sup>GEOPS-Geosciences Paris Sud, CNRS, Université Paris-Saclay, Orsay, France, <sup>9</sup>Institute for Computational Cosmology, Department of Physics, Durham University, Durham, UK, <sup>10</sup>Department of Land Economics, National Chengchi University, Taipei, Taiwan, <sup>11</sup>Department of Earth Sciences, University of Gothenburg, Gothenburg, Sweden, <sup>12</sup>Research Centre for Astronomy and Earth Sciences, Sopron, Hungary, <sup>13</sup>Institute of Geological Sciences, Polish Academy of Sciences, Wrocław, Poland, <sup>14</sup>Department of Lithospheric Research, University of Vienna, Vienna, Austria, <sup>15</sup>Planetary Science Institute, Tuscon, AZ, USA, <sup>16</sup>Max Planck Institut für Sonnensystemforschung, Göttingen, Germany, <sup>17</sup>Institut für Planetologie, Westfälische Wilhelms-Universität, Münster, Germany, <sup>18</sup>Astrogeology Team, U.S. Geological Survey, Flagstaff, AZ, USA, <sup>19</sup>Institute for Computational Cosmology, Department of Physics, Durham University, Durham, UK, <sup>20</sup>BAERI, Planetary Systems Branch, Space Science and Astrobiology Division, Moffett Field, CA, USA, <sup>21</sup>The Johns Hopkins Applied Physics Laboratory, Laurel, MD, USA

**Abstract** A project of mapping ice-related landforms was undertaken to understand the role of subsurface ice in the northern plains. This work is the first continuous regional mapping from CTX (*ConTeXt Camera*, 6 m/pixel; Malin et al., 2007) imagery in Arcadia Planitia along a strip 300 km across stretching from 30°N to 80°N centered on the 170°W line of longitude. The distribution and morphotypes of these landforms were used to understand the permafrost cryolithology. The mantled and textured signatures occur almost ubiquitously between 35°N and 78°N and have a positive spatial correlation with inferred ice stability based on thermal modeling, neutron spectroscopy, and radar data. The degradational features into the LDM (latitude-dependent mantle) include pits, scallops, and 100-m polygons and provide supporting evidence for subsurface ice and volatile loss between 35 and 70°N in Arcadia with the mantle between 70 and 78°N appearing much more intact. Pitted terrain appears to be much more pervasive in Arcadia than in Acidalia and Utopia suggesting that the Arcadia study area had more widespread near-surface subsurface ice and thus was more susceptible to pitting or that the ice was less well buried by sediments. Correlations with ice stability models suggest that lack of pits north of 65–70°N could indicate a relatively young age (~1 Ma); however, this could also be explained through regional variations in degradation rates. The deposition of the LDM is consistent with an air fall hypothesis; however, there appears to be substantial evidence for fluvial processes in southern Arcadia with older, underlying processes being equally dominant with the LDM and degradation thereof in shaping the landscape.

**Plain Language Summary** We mapped ice-related landforms in Arcadia on the northern plains of Mars. This was the first continuous map at this scale. The maps of these ice related landforms were used to understand the role of ice has in shaping the Martian landscape. We found evidence that suggest that ground ice occurs almost everywhere between 35°N and 78°N. We also found landforms associated with loss of ground ice to be widespread suggesting that Arcadia used to have even more ground ice in the recent past. The pattern of landforms we see suggests that the ground ice is sourced from the air, either as snowfall or direct condensation onto or into the near surface.

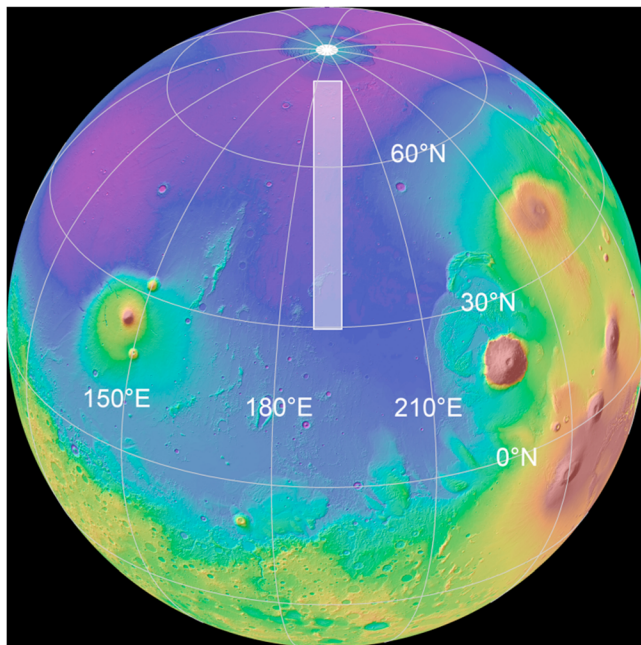


**Figure 1.** Colorized MOLA elevation map showing the location of Arcadia grid mapping strip. Blue colors represent low elevation and red, high.

## 1. Introduction

### 1.1. Northern Plains

The northern plains of Mars cover nearly a third of the planet and comprise several large overlapping basins (Frey, 2006) that are topographically lower than the *cratered highlands* of the southern hemisphere. These basins are variably filled and buried by materials stratigraphically much younger than the majority of the southern highlands (e.g., Tanaka et al., 2005; Taylor Perron et al., 2007). The region has been proposed to have once hosted an ancient ocean (e.g., Baker et al., 1991; Taylor Perron et al., 2007), but the uppermost layers of the northern plains are interpreted to be sediments emplaced by various processes and have since been reworked by *periglacial-like* processes (Tanaka et al., 2005).

Recent measurements of hydrogen abundance in the upper tens of centimeters of the Martian regolith show that the middle to high latitudes of present-day Mars contain significant quantities of water-equivalent hydrogen, inferred to be subsurface ice in both hemispheres (Boynton et al., 2002; Feldman et al., 2004; Wilson et al., 2018). This ice content has been confirmed by many morphological observations, including ice revealed by small impacts (Byrne et al., 2009), thermal contraction cracks (e.g., Levy et al., 2010; Mangold, 2005; Ulrich et al., 2011), lobate/rampart impact ejectas (e.g., Squyres & Carr, 1986), pedestal craters (e.g., Costard, 1989), sublimation pits (e.g., Costard & Kargel, 1995; Morgenstern et al., 2007; Séjourné et al., 2011; Soare et al., 2005), clastic networks and lobes (e.g.,

Gallagher & Balme, 2011), and—perhaps most reliably—remote (e.g., Dundas et al., 2018) and in situ (e.g., Mellon et al., 2009) observations of massive ice.

It is clear that Mars' northern plains include large areas in which sediments have recently been shaped by periglacial processes. However, the ratio between water-ice and sediment in the northern plains is unclear. Determining whether there is excess ice or ice-cemented regolith has important implications as to formation. Excess ice (where ice content exceeds the total pore volume) is likely to have accumulated from the atmosphere, either by condensation within the regolith (e.g., Fisher, 2005; and subsequent ice lens growth; Sizemore et al., 2015) or by niveo-eolian deposition. It is likely that variations in Mars obliquity and/or orbital eccentricity (Laskar et al., 2004) have played a role in creating climate cycles that in turn controlled atmospheric deposition and removal of surface and near-surface ice on Mars (e.g., Head et al., 2003; Mustard et al., 2001). However, ice-cemented regolith could also have been deposited by surface or subsurface processes (e.g., Lucchitta et al., 1986; Mahaney et al., 2004), such as freezing of wet sediments deposited by fluvial, marine, or lacustrine processes (surface; e.g., Soare et al., 2017), or shallow groundwater processes (subsurface). Hence, ice and sediments could have been deposited in the northern plains by a combination of multiple processes or by different processes in different locations. Similarly, the origin of the ice-hosting materials is largely unknown, and many questions remain: are these sediments eolian (dunes or loess), fluvial, lacustrine, marine, or volcanoclastic? Could some regions be near-surface exposures of ancient, deeply weathered lavas?

### 1.2. Arcadia Planitia

Arcadia Planitia is an extensive lowlands region northwest of the Elysium Volcanic region of Mars. It lies north of the Amazonis Planitia region and is separated from Acidalia Planitia to the east by a low topographic saddle and from Utopia Planitia to the west by a similar feature (see Figure 1). North of Arcadia is the north polar region of Mars, comprising the polar cap and circum-polar dune fields of Olympia Undae (see Figure 2). Global-scale mapping suggests that Arcadia Planitia basement material is dominated by Hesperian to Amazonian-aged lavas and sediments (Tanaka et al., 2005) overlying a Noachian basement (e.g., Frey, 2006). The underlying basement is believed to have undergone widespread alteration by liquid water, as implied by phyllosilicate outcrops in the rims of large impact basins (Carter et al., 2010). More recent deposits superpose this basement, and their mapped dielectric characteristics (Mouginot et al., 2012), suggest that the widespread Vastitas Borealis Formation, dominant in northern Arcadia, is, like much of the northern plains

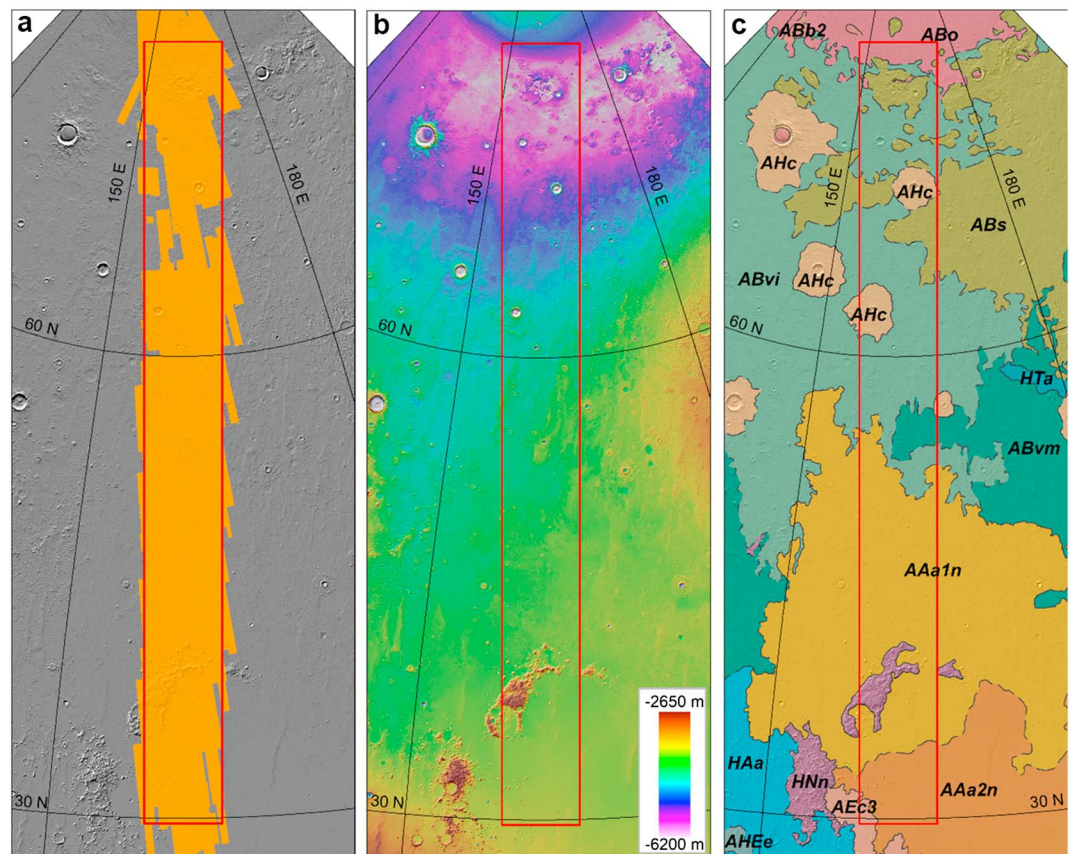


**Figure 2.** Location of Arcadia Planitia mapping strip. (a) CTX coverage within the study area. (b) MOLA topography. (c) Geological map of Arcadia Planitia adapted from Tanaka et al. (2005) overlain onto a MOLA hillshade (Smith et al., 2001). Key units include ABo (Olympia Undae unit—dunes), ABs (Scandia region unit—thick sedimentary deposits with collapse features), ABvi and ABvm (Vastitas borealis interior and marginal units—heavily reworked sedimentary and volcanic materials containing kilometer-scale polygons and *thumbprint* terrains), AAa1n (Amazonis Planitia 1 north unit—surficially modified volcanic materials), AAa2n (Amazonis Planitia 2 north unit—lava flows sourced from Amazonis Planitia or Cerberus Fossae), HNa (Nepenthes Mensae unit—rugged inliers of ancient bedrock), and AHc (impact-crater ejecta).

(Tanaka et al., 2005), composed of low-density deposits and/or subsurface water ice deposits (see Figure 2). These massive units of sediments and water ice are possible remnants of a Late Hesperian ocean (Carr & Head, 2003). The deposits in Arcadia probably also reflect erosion of surrounding uplands followed by transport of fluidized debris into the depocenter to form deposits hundreds of meters thick (Tanaka & Kolb, 2001).

At the northern extent of the Arcadia swath (see Figure 2), the Olympia Undae dune fields display both barchan and transverse forms and contain actively migrating and evolving dunes (Ewing et al., 2010; Hansen et al., 2011) that overlays the landscape visible to the south. South of the Olympia Undae unit are Scandia region units and interior Vastitas Borealis units. The Scandia region unit is a complex of mesas, knobs, and patches of material ranging from a few hundred meters to a kilometer thick (Tanaka et al., 2005), and the Vastitas Borealis unit is an extensive region of ice-rich, fine-grained materials that contains various landforms indicative of the presence of shallow subsurface ice and processes involving reworking of sediments by ice-related processes (e.g., Tanaka et al., 2005). The presence of double-layered ejecta and pedestal craters (Costard, 1989; Squyres & Carr, 1986) in Arcadia suggests the presence of relatively deep subsurface ice, with their raised form being a result of the ejecta blanket protecting the impact site as the surrounding ice-rich terrain downwastes through sublimation (Barlow & Perez, 2003; Kadish et al., 2009).

Within Arcadia Planitia are regions of *thumbprint terrains* (Kargel et al., 1992; Schaefer, 1990; Tanaka et al., 2005): linear to arcuate assemblages of ridges, hummocks, knobs, and cones of enigmatic origin. They have been suggested to form by karstic processes (differential solution of carbonates; Schaefer, 1990) glacial and



glaciomarine (Kargel & Strom, 1992; Lockwood et al., 1992; Rossbacher & Judson, 1981; Scott & Underwood Jr., 1991), tsunami wave propagation (Costard et al., 2017), and multiple episodes of near-surface fluidization, discharge, and eruption (Tanaka et al., 2005). Hectometer to kilometer-scale polygonal networks consisting of intersecting linear troughs, tens of meters deep and up to 1 km wide, are also present. They have been suggested to be a result of convection cells in a catastrophic flood deposit (Lane & Christensen, 2000), contraction of thick, volatile-rich sediments (Buczowski & Cooke, 2004; Lucchitta et al., 1986; McGill, 1986; McGill & Hills, 1992), or the isostatic rebound following loss of a local waterbody or ice mass (Hiesinger & Head, 2000; Pechmann, 1980).

Farther south, where Arcadia Planitia transitions into Amazonis Planitia, are wide plains of probable volcanic origin (see transition into Amazonis Planitia North units; Figure 2), though now buried by late Amazonian, ice-rich mantling deposits (e.g., Kostama et al., 2006; Kreslavsky & Head, 2002; Mustard et al., 2001). Farther south still are geologically recent plains. These include lobate volcanic flow fields and possibly sediments from large-scale lava and water outbursts sourced from the Elysium Volcanic region (e.g., Burr et al., 2002; Keszthelyi et al., 2000; Plescia, 1990, 2003).

The aim of this paper is to provide information on the distribution of landforms in the Arcadia Planitia region of the northern plains of Mars to help constrain the location and origin of ice and sediments (Figure 1). It is one of three similar studies, each located in a different region of the northern plains—the others being Utopia Planitia and Acidalia Planitia—that intend to produce consistent maps of landform distribution and hence to compare and contrast the landscapes seen across the northern plains. Hemisphere-scale maps of the northern plains have been produced at a scale of 1:15,000,000 (Tanaka et al., 2005), but new high-resolution data sets permit increased geological and geomorphological detail to be seen; capturing this detail is an aim of this work. Although broad-scale heterogeneity in surface geomorphology exists within latitude bands, suggesting that regional geology and climate play a dominant role, many details have not been fully investigated. Improving the geological context of the northern plains will help constrain outstanding questions about Martian geological evolution, environmental change, and—if any of the present-day ice in the northern plains was once in the liquid state—perhaps even astrobiology.

We use a grid mapping approach (see section 3.2; Ramsdale et al., 2017) to explore the distribution of landforms in Arcadia Planitia (Figures 1 and 2) that have been associated with ice or water. We aim to explore whether there are any obvious patterns or correlations between the distributions of individual landforms and (i) parameters such as geological unit type, water content of the regolith, elevation, latitude etc and (ii) the other landforms mapped within the study area.

## 2. Method

### 2.1. Study Area

The study area in Arcadia (Figure 2) is a 300-km-wide strip extending from 30° to 80°N latitude, centered on the 170°W line of longitude. The location of the strip was chosen primarily to maximize the availability of CTX (*ConTeXt Camera*, 6 m/pixel; Malin et al., 2007) images. We used CTX as it has near-global coverage and a spatial resolution sufficient to resolve many landforms associated with ice and subsurface ice. We opted to use a Cassini projection (similar to a cylindrical projection rotated by 90°) centered on the 170°W meridian to minimize distortion across the full length of the strip.

### 2.2. Mapping Approach

A full description of the methodology used is provided in Ramsdale et al. (2017), and only a summary is given here. First, a mosaic of map projected CTX images was created in GIS (Geographical Information System) software (ArcGIS 10.1). Additional data such as MOLA (Mars Orbiter Laser Altimeter; Smith et al., 2001) topography, lower resolution global imaging data, and THEMIS (Thermal Emission Imaging System; Christensen et al., 2004) daytime and nighttime mosaics were also included. We then performed reconnaissance mapping, identifying which specific landforms and terrain types would be studied and catalogued; this involved looking for landforms previously associated with water ice to help build a focused list of landforms to map. The Mars northern plains geological map (Tanaka et al., 2005) was used for context, with some small modification made based on our reconnaissance studies.

The study area was divided into a  $15 \times 150$  grid of squares, each 20 by 20 km. In the GIS, a polygon feature-class shapefile was produced, in which each grid square was represented by a single square polygon object. The shapefile was given an attribute table, with a separate attribute for each landforms type to be studied and a unique identification code for each grid square. The CTX images were then systematically examined, grid square by grid square, at full resolution (between 1:10,000 and 1:20,000), in order to identify the landforms. The landforms were recorded as being either *present*, *absent*, or *dominant*. The dominant classification was used when a single landform type covered the entire grid square to such an extent that other landforms would have been obscured. Where relevant, each grid square could also be recorded as *null* (meaning *no data*) or *possible* if there is uncertainty in identification, either when the mapper is unsure of the identification or when the image quality is poor (32/2,250 grids) but there was some evidence to suggest that the landform is present. To compare the occurrence of multiple landforms with respect to latitude or other data sets, the grid mapping data can be grouped into bins where all positive values (dominant, present, and possible) count toward the total frequency or can be kept separate to provide more refined information.

### 2.3. Landform Selection

The suite of landforms identified within the Arcadia strip, and the motivation for mapping these specific landforms, is provided by Ramsdale et al. (2017) but is here summarized. The landforms and surface types selected for mapping were chosen mainly because they have been associated with past or present subsurface ice. These include landforms associated with glacial processes such as viscous flow features (VFFs; Milliken et al., 2003), glacier-like forms (GLFs; Hubbard et al., 2011; Souness et al., 2012). Also included are landforms associated with periglacial processes such as ~100-m diameter polygonally patterned ground, thought to provide evidence for thermal contraction fracturing of ice-cemented permafrost (e.g., Mangold, 2005) scalloped and nonscalloped pits (thought to have formed by loss of excess ice, analogous to thermokarst on Earth; e.g., Costard & Kargel, 1995; Morgenstern et al., 2007; Soare et al., 2005; and expansion of small impact craters; Dundas et al., 2014; Viola et al., 2015), and 10–20-m-scale patterned grounds described as *linear*, *wrinkled*, *brain* and *basketball terrain* (Kostama et al., 2006): textures which we grouped under the class *Textured*. These have all been associated with degradation or in situ modification of an ice-rich sedimentary surface (Kostama et al., 2006).

We also catalogued signatures of infilling and relief softening that provided a topographic indication of a draping unit, such as the latitude-dependent mantle (e.g., Kostama et al., 2006; Kreslavsky & Head, 2002; Mustard et al., 2001). The identification of this surface type is by inference about relief, rather than by direct observation of surface morphology (i.e., the criteria to identify *mantled* in our study are distinct from those to identify *textured*). We also include landforms potentially indicative of thaw, surface or groundwater flow, such as gullies (Hartmann et al., 2003; e.g., Malin & Edgett, 2000; Soare et al., 2014) and channel-like forms (though larger examples were digitized as linear features as part of our reconnaissance mapping).

Other features were mapped that less explicitly related to subsurface ice processes but were included in case their distribution informed the arguments about ice-rich terrains. These include kilometer-scale polygons, thumbprint terrain, large pitted mounds, and small mounds.

The formation mechanism of the thumbprint terrain and associated large pitted mounds or cones is enigmatic and has been interpreted to many different processes. These processes include static ice sheet removal debris (e.g., Grizzaffi & Schultz, 1989), Rogen moraine-underwater glacial push moraine (e.g., Lockwood et al., 1992), mud volcanism (e.g., Davis & Tanaka, 1995), pingos (for the large pitted mound; e.g., Cabrol et al., 2000), and various volcanic and lava/ice interaction features (Bridges et al., 2003; Bruno et al., 2004; Ghent et al., 2012; Plescia, 1980). Gallagher et al. (2018) noted that the distribution, orientation, and extent of pitted cones suggest that they represent widespread underground conduits analogous to volcanic fissure vents or chains of landforms related to hydrovolcanic or cryovolcanic phreatomagmatic eruptions, including rootless cones and mud volcanoes. In this interpretation, each cone being the locus of an upward movement of pressurized liquid carrying and depositing sediment or becoming a solid as it reached the surface. Rootless cones and mud volcanoes are significant because they indicate past interactions between lava and either subsurface ice or groundwater making them of interest to a hemispherical study of subsurface ice-related landforms and are addressed in greater detail in the Acidalia study (REFS).

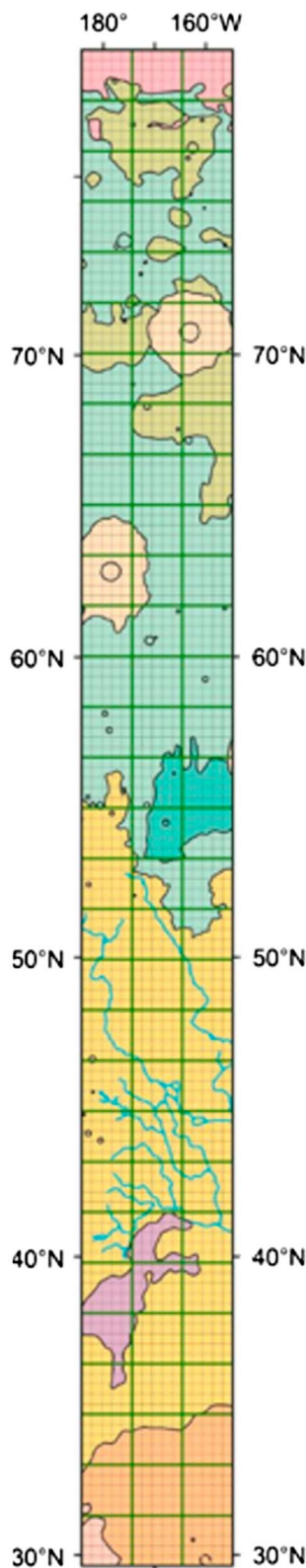


**Figure 3.** Geological map of the study area (see Figure 2 for details) based on Tanaka et al. (2005) with our additions of channel-like forms between 40 and 50°N (blue lines).

Kilometer-scale or giant polygons are thought to be a product of tectonic, volcanic, desiccation, or compaction processes and could be a result of faulting and rebounding following the removal of a water/ice load (e.g., El Maarry et al., 2010; McGill & Hills, 1992; Pechmann, 1980). These kilometer-scale forms were mapped using a combination of THEMIS and CTX, as they could often be more easily seen in lower resolution THEMIS images than high-resolution CTX data.

Reconnaissance mapping revealed the presence of small mounds: typically small, featureless hills less than 30 m in diameter that are morphologically similar to rootless cones (e.g., Lanagan et al., 2001), pingos (Burr et al., 2009), or mesa-like erosional remnants. These were included in case their mapped distributions revealed information that could be used to infer their formation mechanism.

Geomorphic features that may account for the absence of other landforms include dune fields, massive ice (used throughout the manuscript to refer to large masses of ice visible in surface imagery), and continuous *bedrock* formations such as lava flow units devoid of obvious superposing landforms. An example of bedrock is the platy-ridged material inferred to be lava flows in Southern Arcadia/North Amazonis Planitia (Keszthelyi et al., 2000).

#### 2.4. Radar Observations

We analyzed 96 observations from the shallow radar (SHARAD) instrument that cross the Arcadia Planitia swath (digitized figure with radar shapefiles). Each of these radar observations was analyzed for subsurface reflections. All possible detections were recorded and projected into map view to look for spatial correlations. A full description of the methods is available in Smith and Holt (2015). First, a comparison with a simulated radargram was completed to predict where reflections were originating on the surface, both from nadir and to the side. The second step is to identify sidelobes, artifacts of radar processing deconvolution that occur 0.24  $\mu$ s below the surface return and are a lower intensity. Once the sidelobes and clutter could be identified, we distinguished surface reflections from true subsurface reflections. The subsurface reflections represent an interface between contrasting materials and may come from many sources: air regolith, regolith ice, and ice basement. In this grid mapping survey we search only for detection interfaces and provide a likely cause; however, we do not measure the dielectric properties of the materials that create the reflection. The spatial relationships are recorded for each orbital/observation ground track.

### 3. Observations

#### 3.1. Reconnaissance Mapping

The initial reconnaissance study identified those landforms to be mapped during grid mapping and allowed us to check for other features that were not shown in previous small-scale maps (Tanaka et al., 2005, e.g., Tanaka et al., 2014), which might be important in our study area. To represent the local geology in the Arcadia strip, we chose to use the northern plains map of Tanaka et al. (2005). Our reconnaissance showed that the channels were more extensive than portrayed in the northern plains map (understandably, given the different mapping scales and base map resolutions), so these have been overlain onto the otherwise unmodified northern plains map (Figure 3).

### 3.2. Grid Mapping Results: Overview

The results of the grid mapping are shown in Figure 4, which portrays the spatial distribution of all of the mapped landform types. Figure 5 shows the frequency and latitude distribution of all the landforms, grouping all positive identifications (probable, present, and dominant) of landforms and giving them equal weight.

### 3.3. Grid Mapping Results: By Landform

#### 3.3.1. Mantled and Textured

As shown in Figures 4 and 5 approximately 86% of the grid squares contain surfaces that are mantled, textured, or both. Mantled and textured terrains are highly correlated, with 75% of the grid squares in the study area containing both signatures. The trends in abundance by latitude of mantled and textured surfaces are almost uniform between 78 and 35°N. The areas that are mantled but not textured have a smooth appearance and underlying topography appears to be more subdued as shown in Figure 6. The areas that are textured but not mantled are typically flat-lying areas with few high-relief features that could show evidence of mantling. These observations are consistent with the presence of a ubiquitous draping unit mantle that has been degraded to form the textured appearance.

#### 3.3.2. Pitted

Pitted surfaces appear across the study region in the areas 60–68°N and 36–56°N. There is a significant *gap* between 56 and 60°N. The pitted texture comprises circular to irregular and often overlapping depressions tens of meters across (see Figure 7), but there is clearly an overlap between complex pits and scalloped depressions. The pitting occurs most often on mantled and textured surfaces, supporting the hypothesis of a degrading mantle. The region between 70 and 80°N shows few pits, although the surface still shows both textural and topographic mantle signatures. This suggests that the mantling unit is undegraded.

#### 3.3.3. Scalloped Depressions

The individual scallops in Arcadia are around a few hundred meters across with cusped edges, like those found in Utopia (Costard & Kargel, 1995; Morgenstern et al., 2007; Séjourné et al., 2011; Soare et al., 2007; Ulrich et al., 2010), and they show consistent asymmetry with steep poleward facing scarps on their southern boundary (see Figure 8). However, whereas individual Utopian scalloped depressions can often be clearly delineated (see Séjourné et al., 2011), the scallops in Arcadia often have no obvious northern edge (see Figure 8). Figure 8 also shows that the area around the scalloped terrain is often pitted by more roughly circular depressions, making identification difficult. Overall, the grid mapping shows that the identification of scalloped depressions is tentative in Arcadia and occurs only in a narrow band between 50 and 55°N. However, even given that there is potential for crossover in identification between scalloped depression and *pits*, what is clear is that scalloped terrains are much less prevalent in Arcadia than the large assemblages described in Utopia Planitia (Séjourné et al., 2012, 2018).

#### 3.3.4. Large Pitted Mounds

When identifying large pitted mounds, we were looking for specifically kilometer-scale hills with a summit depression (see Figure 9a). Large pitted mounds are found in <1% of the Arcadia strip, and putative examples lack the distinct albedo contrast of the *type examples* seen in Acidalia Planitia (Orgel et al., 2016). However, given that the features identified are also in regions that are recorded as mantled, the albedo contrasts could be subdued by this materials leaving morphology as the only indicator. Hence, identification of large pitted mounds was often tentative and with low certainty of correct identification. For example, it is likely that at least some of the large pitted mounds identified in are likely to be degraded and buried impact craters (Figure 9b; also Buczkowski et al., 2005).

#### 3.3.5. Small Mounds

Cone or dome-like, isolated small mounds were included in the survey because of their morphological similarity to various ice-related landforms (e.g., pingos and rootless cones). The area between 35 and 55°N displays many such mounds, each approximately 100 m in diameter, smooth in appearance, and with no obvious features or textures in either CTX or HiRISE images (see Figure 10). There is no obvious difference in the albedo or color between the mounds and the surrounding material. Even where they do occur, the mounds have low spatial densities, with roughly <10 to a few tens of mounds per 20-km by 20-km grid square.

#### 3.3.6. The 100-m Polygons

Two groups of 100-m-scale polygons can be observed in the Arcadia strip (see Figures 4 and 5), but observations are sometimes tentative and morphologies uncertain. The southern groups of polygons found between



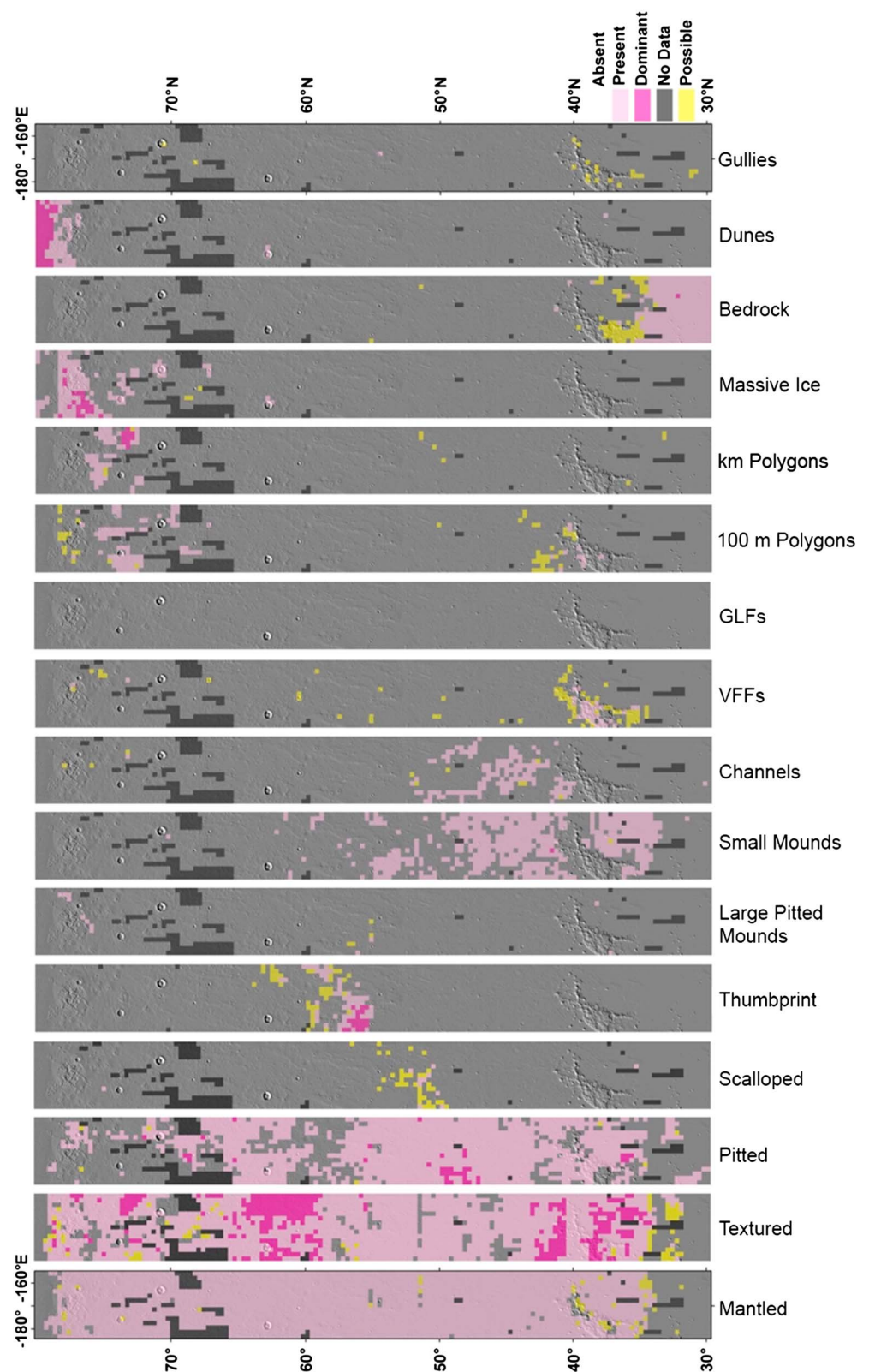


**Figure 4.** Grid mapping results from Arcadia. Landforms were recorded as being either present (color—light pink), absent (color—white/transparent is where underlying hillshade is more visible), or dominant (color—dark pink) null (color—gray; meaning no data) or possible (color—yellow). Background is a MOLA hillshade, lighting toward the southeast.



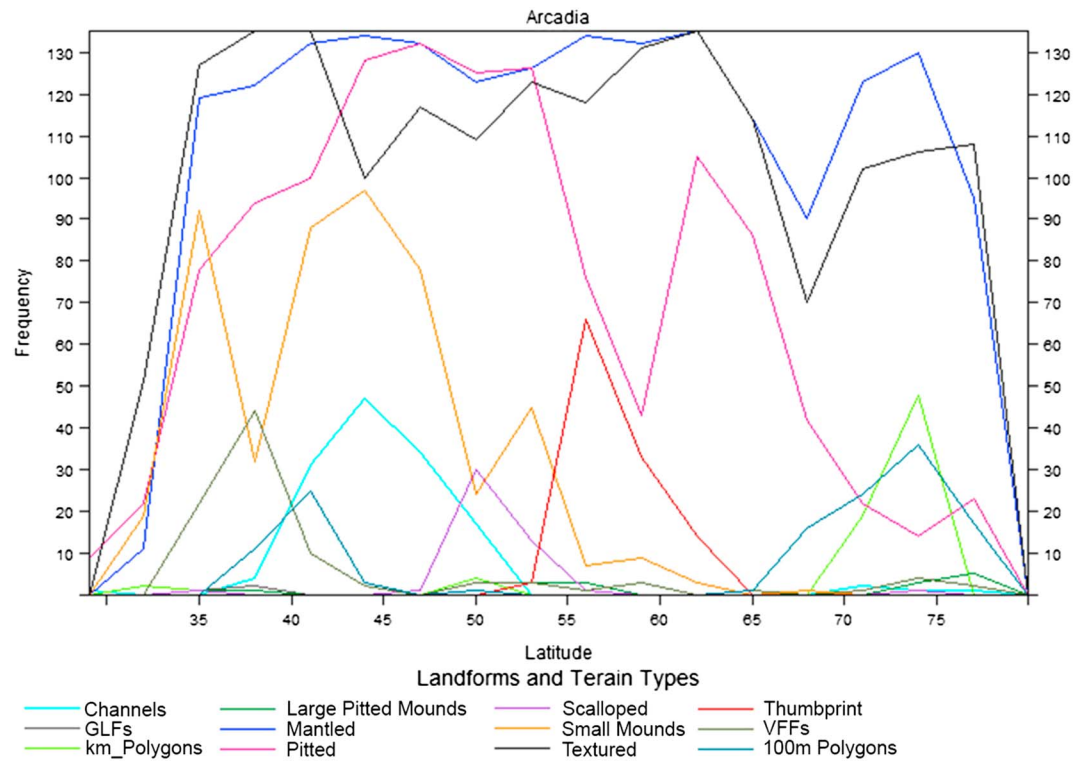


**Figure 5.** Frequency of landform occurrence by latitude in the Arcadia strip.

38 and 45°N are generally angular, irregular, high-centered features (see Figure 11a). These southern polygons have clear topographic steps and appear more like bedrock fracture networks rather than obvious subsurface ice-related features. The northern groups of polygons found between 66 and 78°N are generally characterized by high-albedo boundaries with dark centers (Figure 11b). These northern polygons are reminiscent of frost-filled thermal contraction cracks, but again, their morphology is often unclear. What is clear, however, is that there are many fewer 100-m-scale polygons visible in Arcadia than smaller polygonally patterned grounds (seen as part of the textured category) and far fewer than mapped in the Acidalia and Utopia areas (Orgel et al., 2018; Séjourné et al., 2018).

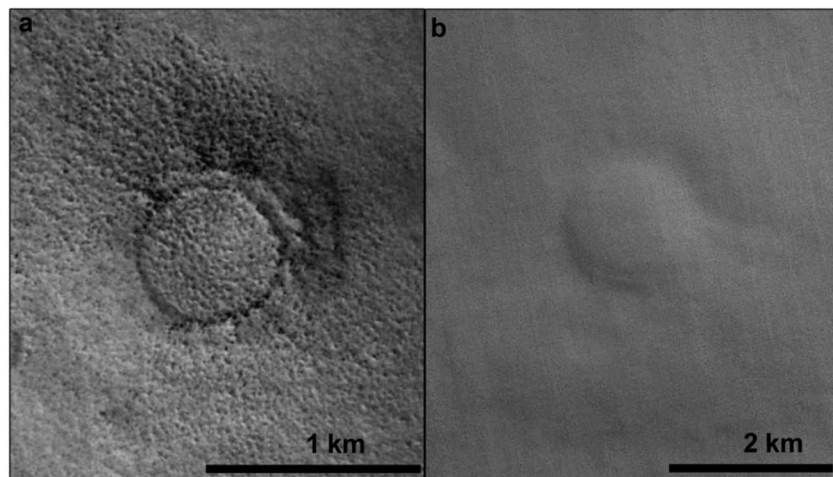


**Figure 6.** (a) CTX image P17\_007696\_2568 showing a mantled and textured surface. (b) CTX image P16\_007248\_2558 a mantled but not textured surface. In this case, the identification of textured is hampered by image quality, or the textured appearance is either absent, or at a scale too small to see in CTX data.

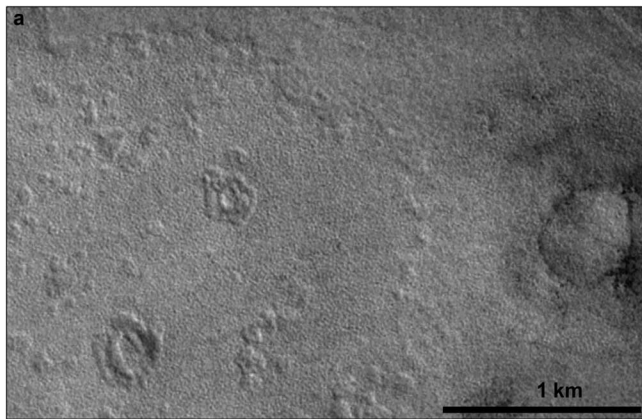


**Figure 7.** CTX image P16\_007248\_2558 showing a pitted texture.

### 3.3.10. Thumbprint Terrain

Thumbprint terrain in the Arcadia grid mapping occurs only between 55° and 65°N and is composed largely of kilometer-scale ridges (Figure 12a). It was generally identified in THEMIS imagery—being less prominent to see in CTX data. It is smoother than the conical chains that comprise the thumbprint terrain in Acidalia and Utopia (Orgel et al., 2018; Séjourné et al., 2018) but, as shown by the grid mapping and higher-resolution observation (Figure 12b), is clearly overlain by mantle and textured signatures, suggesting that the thumbprint terrain is buried in Arcadia.

### 3.3.11. Kilometer-Scale Polygons

Kilometer-scale polygons occur between 72 and 76° N (Figures 4 and 5). They form in clusters, are high-centered with rounded edges, and form irregular, nongeometric shapes 1–3 km across. Detailed observations confirm that these features are not related to mantling deposits but form in bedrock: multiple impact craters can be seen that occur in the kilometer-scale polygon and which have been mantled by textured surface materials. This shows that these large polygons relate to submantle geology, predating the mantle emplacement (see Figure 13).

### 3.3.12. Channels

Channels were included in the grid mapping scheme in order to search for possible fluvial systems too small to be visible in low resolution data, or mappable in small-scale global-to-regional studies. However, we also mapped fluvial features as part of the reconnaissance mapping, delineating a large channel system between 35–50°N and 150–175°W. All the *channel* identifications in the grid mapping relate to this system.

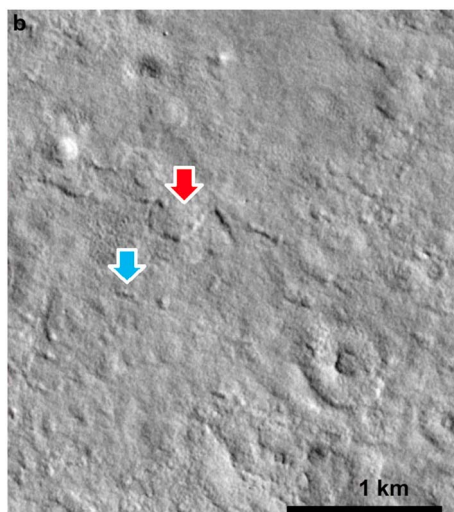


**Figure 8.** CTX image G03\_019221\_2327 showing the morphology of scalloped terrain (e.g., red arrow—i.e., not to be confused with pitted terrain, e.g., blue arrow) in Arcadia Planitia.

### 3.3.7. VFFs

VFFs are largely restricted to one small area within the Arcadia strip between 35 and 42°N. The VFFs are all Lobate Debris Aprons (Milliken et al., 2003) or similar features that form around inliers of ancient bedrock that form the Nepenthes Mensae unit. Other examples of VFFs in Arcadia include putative Lobate Debris Aprons around topographic highs and concentric crater fill, but these observations are tentative and rare within the Arcadia strip.

### 3.3.8. GLFs

No reliable identifications of glacier-like forms were made in the Arcadia strip.

### 3.3.9. Gullies

No convincing evidence for gullies was found in the Arcadia strip in our mapping, although higher-resolution images might reveal a small population.

Given that these channels systems are of significant extent, we extended our mapping slightly to characterize the network better. This is shown in Figure 14a and reveals a branching network, connecting a dark feature to the southeast of the study area (X) to another to the west of the study area (Y), with multiple small branches opening the north and west. Assuming that the systems formed by downhill flow of a fluid and that the topography has changed little since emplacement, topographic profiles suggest the system to be distributary, flowing from southeast to north or northwest (see Figure 14b) with continuous sections 500–1,000 km long. Close study shows that the channels are darker than the surrounding material and range in width from tens of meters to several kilometers. The channels are mostly simple and sinuous or sublinear (Figure 14d), but in some regions they appear to be anastomosing or braided (see Figures 14a and 14c). Cross profiles of the channels (Figures 14b and 14c) show various sectional morphologies, from V and U shaped to ridged, and they are at most typically 20–30 m in depth. The channels appear to originate from a low-albedo region, but when studied using HiRISE and CTX data, no obvious vent or origin for the fluid that formed the channels can be seen, and the source area instead appears to be flat lying.

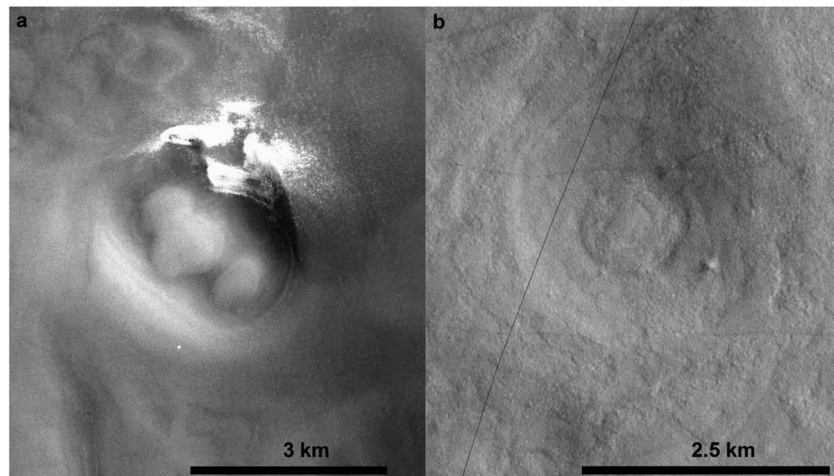


**Figure 9.** Large pitted mound candidates. (a) Mound with possible summit depression in CTX image P21\_009318\_2572. (b) Low-confidence candidate that could be a buried and degraded impact crater in CTX image P21\_009305\_2377.

Most channel sections narrow with distance and terminate abruptly. However, two channel sections terminate at a low-relief, low-albedo region (see Figure 15) that is similar to the source region (assuming downhill flow). The channels, source, and terminations appear bright in both day and night THEMIS images indicating that they are composed of a material with higher thermal inertia than the surrounding material. This higher thermal inertia suggests that the channels contain coarser or more indurated material (e.g., Ferguson et al., 2006) than the surroundings.

### 3.3.13. Massive Ice

Massive ice in the Arcadia grid mapping area includes polar cap outliers found between 72 and 80°N and ice deposits around the rims of large impact craters—found as far south as 60°N. They range in size from tens of meters across to few hundred kilometers across. The massive ice deposits are easily identified by their high-albedo and smooth uncratered surfaces.

### 3.3.14. Bedrock

Surfaces mapped as *bedrock* become dominant south of 35°N. These bedrock areas correlate with platy-rigged material inferred to be lava flows (Keszthelyi et al., 2000, 2004; Plescia, 2003). The transition between the bedrock signature and the textured and mantled signatures appears to be gradational rather than a

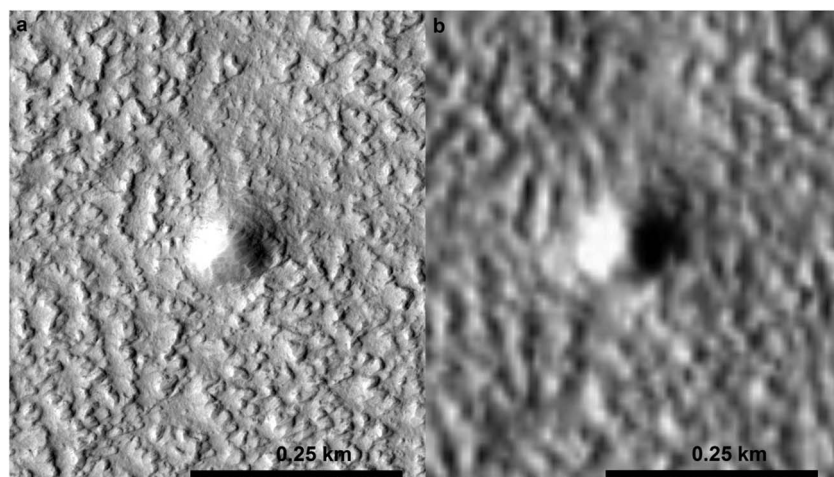


**Figure 10.** (a) HiRISE image ESP\_026856\_2160 of a small mound at 25 cm/pixel. (b) CTX image G22\_026856\_2148 showing the same small mound at 6 m/pixel as it appeared in our grid mapping. The small mound is around 100 m across and surrounded by textured terrain.



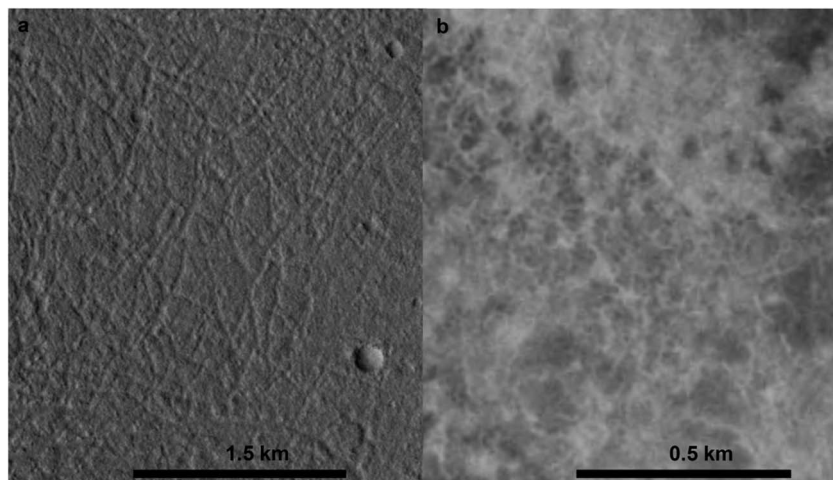


**Figure 11.** (a) CTX image P16\_007433\_2181 showing high-centered 100-m-scale polygons from the southern set in Arcadia. (b) CTX image B18\_016531\_2540 showing high-albedo contrast 100-m-scale polygons from the northern set in Arcadia.

distinct boundary, as shown by platy-ridge material that has softened edges and textural signatures in the interridge zones (Figure 16).

### 3.3.15. Dunes

The northernmost part of the strip overlaps the Olympia Undae unit, so dune fields dominate between 76 and 80°N. Individual dunes are tens to hundreds of meters across and up to several kilometers in length. The dunes tend to have crisp edges and appear not to be mantled. The surrounding surfaces are particularly smooth, lacking textured signatures. Impact craters found in these interdune areas tend to be subdued, suggesting that a relatively undegraded mantle underlies the dunes.

### 3.4. Identification of Landforms for Further Analysis

We now focus our analysis on those landforms we believe most able to address the distribution, origin, and role of subsurface ice in shaping the northern plains. Of the landforms mapped, some overlie *geologically recent* ice-related materials (dunes and massive ice), and others are clearly superposed by them and show no correlation with other data sets (kilometer-scale polygons, thumbprint terrains, and bedrock). We do not consider any of these terrains further, although they are clearly of wider scientific interest. Also, the channels signature appears to be better described by the reconnaissance mapping, so we do not consider this result further (at least in terms of the channels grid mapping result). VFFs, GLFs, large pitted mounds, and gullies are rare in the study area or are easily explained by their setting (VFFs in rugged areas, for example), so we also do not consider these any further. In the next section, therefore, we consider the distribution of the following signatures: mantled, textured, pitted, scalloped depressions, 100-m polygons, and small mounds. We compare their distributions with one another and with other parameters.

## 4. Comparison With External Parameters

To help understand the controls on certain landforms, we compare their distributions with the following data sets: elevation, roughness, regional geological unit, thermal inertia, water content of the near-surface regolith, RADAR-observed subsurface reflectors, and theoretical models of subsurface ice distributions. We aimed to select data sets most useful for this study, to provide illustrative results that demonstrate the utility of the approach.

### 4.1. MOLA Elevation and Roughness

To evaluate elevation, we have calculated the mean values of MOLA gridded terrain pixels within each grid mapping square for comparison with the landform distributions. We also calculate a MOLA-derived *surface area* in each grid square (i.e., the size of the 3-D surface created by the relief within the grid square), which serves as a proxy for roughness (flat areas will have a surface area equivalent to the plan view grid square



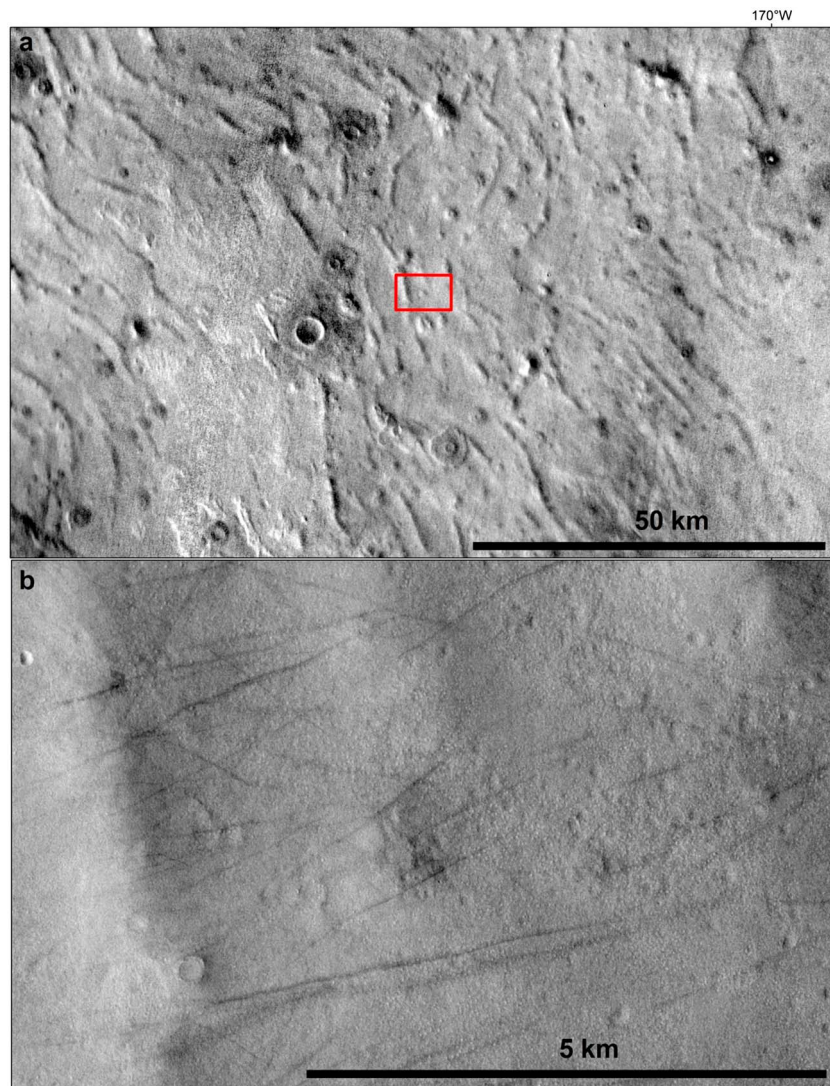


**Figure 12.** (a) THEMIS daytime infrared showing thumbprint terrain; red outline shows location of (b). (b) CTX image P21\_009305\_2377 showing both pitted and textured signatures overlying the thumbprint terrain.

area, and rougher areas have a much larger 3-D surface). Roughness generally decreases from north to south and is lowest in the far south (coincident with bedrock regions in grid mapping) and highest in the Nepenthes Mensae unit areas that are associated with rugged inliers of Noachian terrain (see Figure 17). Local regions of higher roughness are associated with impact craters and their ejecta blankets. There is a significant change in roughness at the north-south landform-type boundary marked by the thumbprint terrain, suggesting that the thumbprint terrain might be either a topographic boundary physically dividing different processes or is serendipitously situated at a change in physiography.

The topography grades gently from  $\sim -3,000$  m in the south to  $\sim -6,000$  m in the north (see Figure 17). This makes it difficult to determine whether landforms are topography dependent or latitudinally dependent based on our data. However, viscous flow features are concentrated in areas with higher elevation and roughness as expected, as they occur on or near steep slopes (see Figure 17). Areas with channels and small mounds appear to be confined to a much flatter and less varied surface than the landforms found to the north (Figure 17). From the grid mapping alone, the causal relationship is not clear, but it could be that either (i) the processes that formed the channel and small mound assemblages infilled, or planed the topography thereby removing relief, or (ii) that the processes that form these landforms are slope dependent, forming only on low-relief areas, or (iii) that processes found outside this region themselves create slopes and increase surface roughness.

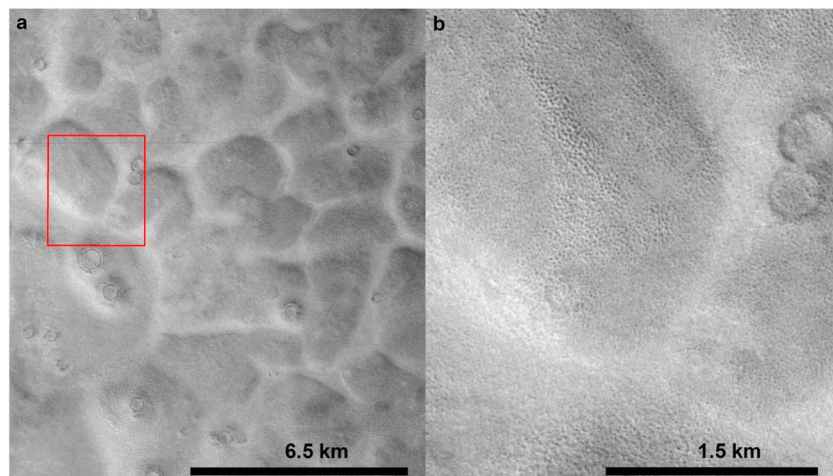


**Figure 13.** (a) CTX image G23\_027251\_2528 showing high-centered kilometer-scale polygons in Arcadia; red outline shows location of (b). (b) CTX image G23\_027251\_2528 close-up of a kilometer-scale polygon. Note the textured appearance and the mantling of impact craters.

Some landforms appear to be confined to tight elevation constraints (e.g., thumbprint terrain from  $-4,300$  to  $-4,000$ ). However, given that these landforms also occur within a tight latitude band and are clustered in one location, it is difficult to determine if they are controlled by topography, latitude, or neither of these. We note that in some other regions, thumbprint terrain forms at different latitudes and elevations (Skinner et al., 2012). Landforms found in the south of Arcadia are naturally at a higher elevation than those found in the north, given the topographic gradient over the study area.

#### 4.2. Geology

The mantled, textured, and pitted landforms appear to cover all mapped geological units ubiquitously, consistent with what would be expected from a recent latitude-dependent mantle. The channels and small mounds and—to some extent—scalped depressions fall largely within the geological units Amazonis Planitia North 1 and 2 as mapped by Tanaka et al. (2005). Their interpretation for the Amazonis Planitia units is of voluminous lava and volcaniclastic flows, suggesting that the infilling of topography is the most likely explanation for the low roughness and slope values in the southern extent of the strip. This leads to the questions as to the origin of the sediments in which the scalped depression form, and whether the channels and small mounds might be related to volcanic, as opposed to fluvial processes. Bedrock signatures in Arcadia match almost exactly the extent of platy-ridge material (Keszthelyi et al., 2000) mapped as the Cerberus Fossae units in the northern plains map of Mars (Tanaka et al., 2005). The mapped dunes correspond with the Olympia Undae unit (Tanaka et al., 2005) and, as expected, form part of large dune field at the northern end of the strip. Small mounds, channels appear to be found mainly within the Amazonis Planitia 1 north unit. No other clear relationships between geology as mapped by Tanaka et al. (2005) and grid mapping of landforms can be seen.

#### 4.3. Thermal Model Results

Chamberlain and Boynton (2007) modeled the depth to conditions that could support stable subsurface water ice and the effects of cyclic changes in Mars' obliquity (Laskar et al., 2004) that have been inferred to control recent ice deposition and degradation cycles on Mars (Head et al., 2003). The mapped extent of mantled and textured terrains correspond very well with predictions for the stability for subsurface ice below 1-m depth at obliquities close to present ( $25^\circ$ ) conditions (Chamberlain & Boynton, 2007), consistent with the hypothesis that there is climate-dependent control of subsurface ice. Their prediction of stable subsurface ice even at lower obliquities for the northern extent of this area is consistent with the observations that the mantling deposits appear thicker, and there is more smoothing of topography, farther north in the strip. North of  $50^\circ\text{N}$ , climate models (e.g., Chamberlain & Boynton, 2007) predict that this ice could be found under stable conditions within 1 m of the surface, but at lower latitudes the ice would be expected to be unstable (see Figure 17d). However, it is important to note that for almost the entirety of the mapping strip, subsurface

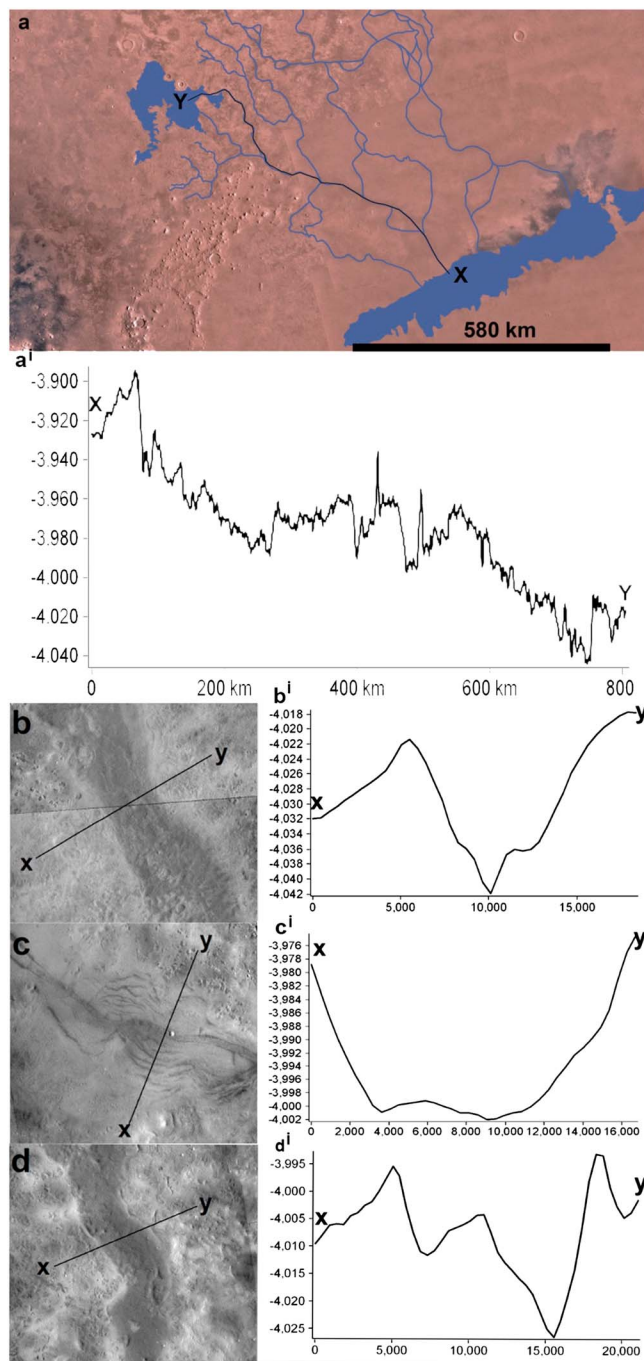


**Figure 14.** (a) Viking image showing the location of (a') example channel long profile (X-Y) and channel system (blue). (b-d) CTX image showing channels and location of (b'-d') cross profiles (X-Y). (b) Located at 46°N and 170°W, (c) located at 47°N and 167°W, and (d) located at 45°N and 168°W.

is not expected to be stable within the uppermost few centimeters and therefore we might expect to see degradation of ice-related landforms. These predictions agree with the measurement of textured and pitted terrains being widespread, but particularly dominating, within middle and lower latitudes. Interestingly, pitted signatures, probably indicative of degradation of ice-supported sediments, are pervasive up to a latitude of about 65–70°N. This matches the Chamberlain and Boynton (2007) ice stability range for obliquities of around 15–20°. This suggests that the mantling materials present here were deposited in a time period during which the obliquity has not been lower than 15–20°, that is, within the last ~1 Ma (Laskar et al., 2004), or that subsurface in the northern plains has been sufficiently shielded as to survive long periods of obliquity driven instability.

#### 4.4. Water-Equivalent Hydrogen (WEH)

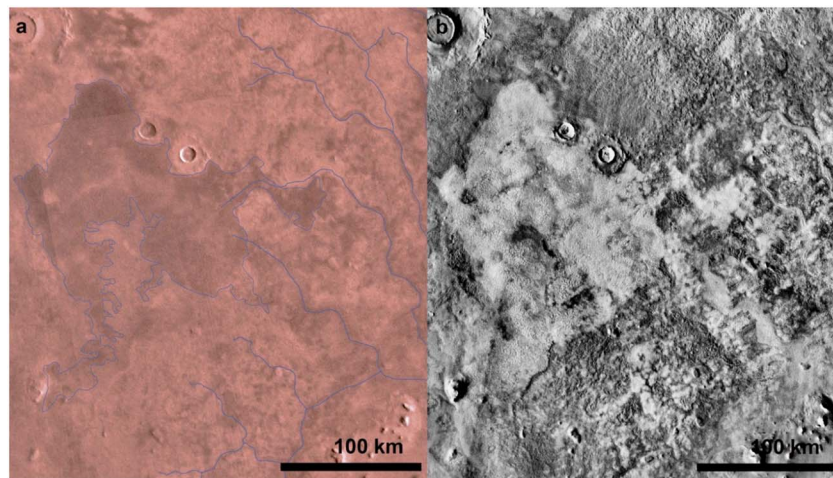
The results of the Mars Odyssey Neutron Spectrometer (MONS) reveal significant quantities of hydrogen (almost certainly in the form of water ice rather than hydrated minerals) in the near surface within the Arcadia strip, supporting the hypothesis of a ubiquitous, layered sediment, and water ice mantle (Boynton et al., 2002; Feldman et al., 2002; Wilson et al., 2018). The nonzero values over almost the entire length of the strip, but with an obvious gradient of more water/ice in the north, and less water/ice in the south, together with widespread pit development, are supportive of the hypothesis that there has been widespread loss of subsurface ice in the northern plains. Further study into size and density of pit formation in Arcadia would be required to determine whether the intensity of WEH and/or pitting is dependent on latitude. Alternatively, as MONS is only sensitive to the top 50 cm to 1 m (Boynton et al., 2002; Feldman et al., 2002; Wilson et al., 2018), the gradient could also be explained by progressively thicker lag deposits from north to south. The low WEH values at the very north of strip are expected, as the dunes there are likely to mask any underlying subsurface ice and their surfaces are relatively ice free. Given that the WEH shows a gentle gradient from north to south, it is difficult to say whether any landforms occur only within a specific WEH band from this strip alone.

Figure 17e shows that kilometer-scale polygons correlate with areas with the highest WEH values. While this could indicate that they formed by subsurface ice related processes, they seem to be covered by a significant and largely intact mantle that could be responsible for the high WEH values and as the MONS that produced the WEH values is only effective <1-m depth it is unlikely that these values correlate with the formation of kilometer-scale polygons, which are largely buried by mantle. At first glance, it may appear counterintuitive that massive ice does not have the highest WEH values but this is likely due to proximity with the dune fields, which appear to be largely ice free; many of the cells that contain massive ice also contain dune fields, moderating the low-resolution (approximately 290 km; see Wilson et al., 2018) WEH data.

#### 4.5. Radar

In Figure 17b, we show where we have found radar detections in our mapping survey. Red lines indicate locations where we see subsurface interfaces that correspond to previously detected lava-lava beds (Campbell et al., 2008). Blue lines highlight where we have found reflections that have been previously associated with ice-regolith interfaces (Bramson et al., 2015). As expected the red lines correlate with where we found bedrock to occur and likely represent layers of the platy-ridge material mapped as the Cerberus Fossae units





**Figure 15.** (a) Viking and (b) THEMIS day images of channels and terminations. It is worth noting how the channels in the northeast appear to peter out, whereas the channels in the northwest terminate at what appears to be an area of ponding.

(Tanaka et al., 2005). The blue lines, inferred as ice-regolith interfaces, correlate with the area we found to contain channels and small mounds. These reflections likely represent interfaces between the heavily degraded LDM and the underlying channelized deposits. Large areas of Arcadia were shown to contain excess water ice (Bramson et al., 2015) suggesting that the ice was likely accumulated from the atmosphere. As to whether the ice is sourced entirely from the LDM or whether there has been a significant fluvial source of volatiles within the channelized deposits and where there is a lower ice to sediment ratio is unclear. It is interesting that we do not see more radar reflections in northern Arcadia; combined with widespread and visually thick LDM deposits, we infer that the radar is unable to penetrate deep enough to find the interfaces with the underlying basement. Furthermore, it is only as the LDM is degraded and thins toward the south that we start to see radar interfaces between the LDM and the underlying material.

## 5. Discussion

### 5.1. Aggradation of Ice-Supported Materials

The mantled signatures form an almost ubiquitous surface unit, irrespective of topography, geology, surface roughness, or thermal inertia, and are inferred to represent a latitude-dependent mantle. Due to its

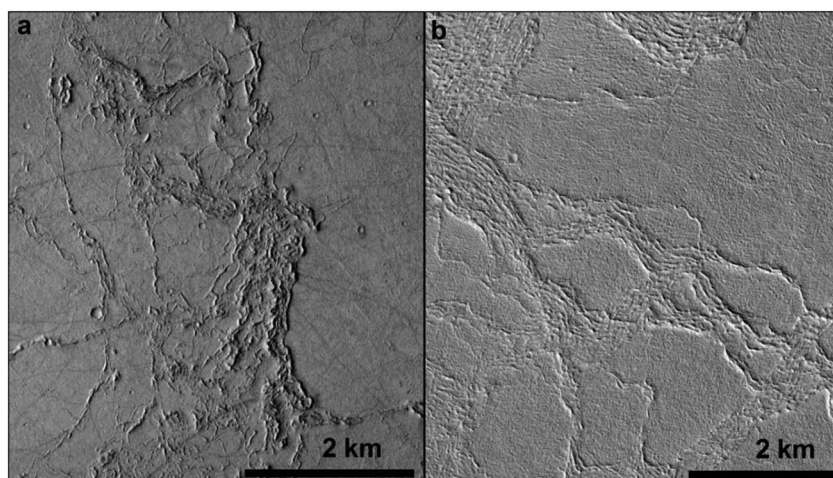


**Figure 16.** (a) CTX image B19\_017151\_2116 showing unmantled/untextured platy-ridge material. (b) CTX image P15\_006866\_2147 platy-ridge material with a softened appearance and a textured signature.



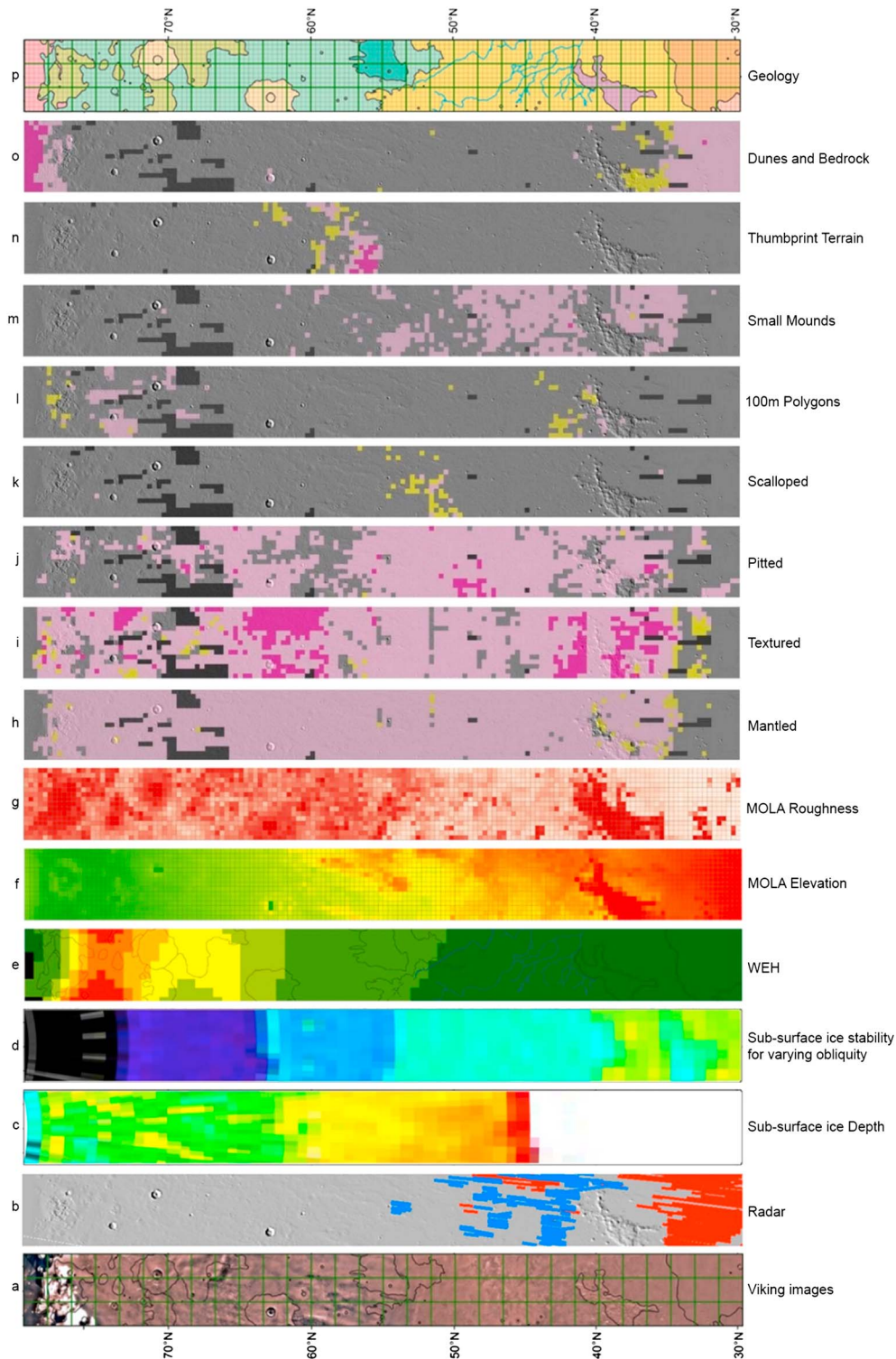


**Figure 17.** (a) Viking image mosaic. (b) Radar subsurface reflections associated with subsurface ice and regolith interfaces (blue) and associated with lava flows (red). Thermal model results for (c) depth to subsurface ice at present and (d) subsurface ice stability at varying obliquities (from Chamberlain & Boynton, 2007). (e) Water-equivalent hydrogen (WEH) in uppermost meter (see Wilson et al., 2018). (f) Gridded mean MOLA elevation. (g) Gridded mean MOLA roughness. Grid mapping results for (h) mantled terrain, (i) textured terrain, (j) pitted terrain, (k) scalloped terrain, (l) 100-m polygons, (m) small mounds, (n) thumbprint terrain, and (o) dunes and bedrock combined. (p) Geological map adapted from Tanaka et al. (2005) with additional channels marked in blue.

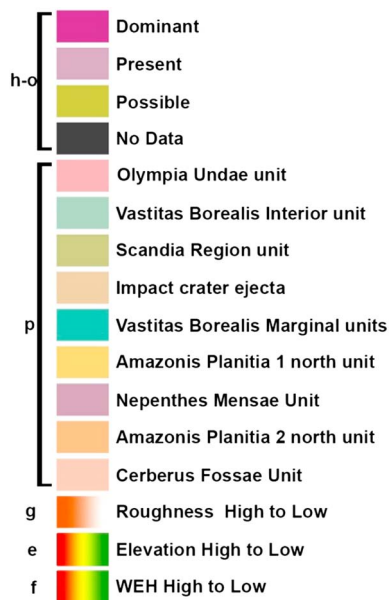


Figure 17. (continued)

widespread textured and pitted appearance, this mantle is thought to contain volatiles (probably water ice) north of 60°N that were largely lost by sublimation south of 60°N (Mustard et al., 2001). This study provides the first continuous mapping of these landforms at full CTX resolution and shows that these terrains occur ubiquitously north of 35°N in Arcadia. The latitudinal gradation among (i) the mantled and textured terrains, (ii) the nonmantled and nontextured bedrock, and (iii) the gradation from high WEH values in the north to low WEH values in the south suggests that the water ice within the LDM is more intact in the north, more having been lost by sublimation in the LDM close to 40°N.

### 5.2. Degradation of Ice-Supported Materials

Widespread pitting supports the idea that the LDM has at least in the past contained volatiles (e.g., Kostama et al., 2006; Kreslavsky & Head, 2002; Mustard et al., 2001) and has been subjected to subsequent volatile loss between 35 and 75°N. Scalloped pits are found between 50 and 55°N but are much less pervasive than in Utopia Planitia (Séjourné et al., 2018). The degradation of the LDM appears to grade from less severe in the north to more severe in the south, with pitting becoming more widespread and more bedrock being observable in the south. Simple correlations with ice stability models (Chamberlain & Boynton, 2007) suggest

that lack of pits north of 65–70°N could indicate a relatively young age as ice would be unstable at these latitudes under 15° obliquities (~1 Ma Chamberlain & Boynton, 2007; 0.4 to 2.1 Ma, Schon et al., 2012) and likely to result in degradation features. Although this neglects the more subtle likelihood that degradation is also dependent on regional climatic conditions and processes that may increase or decrease rates of removal of the ice, rather than simple latitude and topography. Such processes could include, but are not limited to, (i) deposition or removal of eolian dust, which could slow or hasten sublimation; (ii) the permeability, porosity, composition, and percentage ice content of the near-surface material; (iii) regional variations in near-surface humidity, which might control sublimation rate; and (iv) regional variations in insolation due to slope aspect, albedo, thermal inertia, and the resulting surface and near-surface temperatures.

Scalloped depressions and 100-m-scale polygonal fracture networks are far less common in Arcadia than in Acidalia or Utopia Planitiae. The area immediately south of the scalloped terrain in Arcadia is heavily channeled. Such channels are not apparent in the other regions, so it is possible that the scalloped terrain previously extended farther south and has been removed through the process that formed the channels. Alternatively, the surface materials south of 50°N in Arcadia may not be susceptible to scallop formation, whether due to different mechanical properties or percentage water ice content. The scallops of Arcadia are poorly formed in comparison with those found in Utopia. The scallops in Arcadia do not display the inter-depression polygons described by (Séjourné et al., 2011) supporting a hypothesis of less prevalent conditions for scalloped pit formation in Arcadia. This could be result of shallower subsurface ice or a shorter window of prevalent conditions for formation. The same is true for the 100-m-scale polygons, inferred to form by thermal contraction cracking. Taken together with the observation of widespread pitting, these observations could indicate that the surfaces in Arcadia have or had shallower but more widespread subsurface ice content, contain sediments more resistant to degradation (perhaps formed from more competent materials), or have been exposed to environments that are less favorable to loss of subsurface ice, than the other two study areas in Acidalia and Utopia.

### 5.3. Glacial Ice

VFFs and GLFs are landforms indicative of past or present debris-covered or debris-rich ice bodies. They form due to flow and deformation due to gravity, flowing from high to low elevation, and, as such, require relief, either as basement topography or by uneven buildup of ice, creating relief. Thus, their distribution is dependent on regional topography and the latitudinally controlled ability of surface or near-surface to form and remain stable. We found VFFs and GLFs to be primarily concentrated in the 35–42°N band in Arcadia and 40–53°N in Acidalia. This agrees with the proposed 30° to 60° latitude limits from

previous studies (Head et al., 2010; Milliken et al., 2003; Souness & Hubbard, 2012; Squyres & Carr, 1986). As expected, VFFs occur in areas with MOLA-scale roughness (Milliken et al., 2003; Souness & Hubbard, 2012). While VFFs are indicators of the presence of surface or near-surface ice, the absence of VFFs can only be inferred to be an indicator of a lack of near-surface ice in areas of high relief protected from sublimation by a thick lag of dust or debris in areas of less relief; no such inference can be made (Forget et al., 2006; Levy et al., 2009; Page et al., 2009; Souness & Hubbard, 2012). As GLFs are found in only around 0.1% of the grid squares in Arcadia, Utopia, and Acidalia combined, they are not a major indicator for near-surface on the northern plains.

#### 5.4. Volatile-Linked Larger-Scale Landforms

Thumbprint terrain, kilometer-scale polygons, and large pitted mounds appear to occur independent of latitude, topography, and WEH values across the three study areas (REFS). In Arcadia, they appear to be mantled, confirming that they reflect underlying regional geology rather than surficial processes. The thumbprint terrain has been suggested to relate to glacial sediment transport and deposition (Guidat et al., 2015; Kargel et al., 1992; Lockwood et al., 1992; Rossbacher & Judson, 1981; Scott & Underwood Jr., 1991; Tanaka et al., 2005), but the lack of other glacial landforms makes this hypothesis seem unlikely. Whether the thumbprint terrain and large pitted mounds are a relic of large-scale glaciations, or a product of soft sediment deformation and mudflows (e.g., Costard et al., 2015), they do not appear to be indicative of the presence of recent subsurface ice but rather are buried by the LDM in Arcadia. While the exact origins of the kilometer-scale polygons remain enigmatic, the hypotheses involving regional tectonics, sediment deformation, and large-scale dewatering during compression appear likely candidates and again are not indicative of subsurface ice processes but also likely buried by the LDM.

However, the regions with thumbprint terrain present demarcate a boundary between different landform assemblages: south of the thumbprint terrain ( $\sim 60^\circ\text{N}$ ) there is a terrain assemblage of channels (shown by reconnaissance mapping), scallops, and small mounds (see Figures 4 and 5), but these are lacking farther north. North of the thumbprint terrain we see a different set of landforms including kilometer-scale polygons, large pitted mounds (rarely), massive ice, and dunes (see Figure 5). It is possible that the thumbprint terrain provided a topographic barrier to the channel-related landform assemblage, although without a longitudinal extension of the study area, this cannot be determined.

#### 5.5. Channels and Small Mounds

The small mounds in Arcadia do not appear to be directly indicative of subsurface ice. The small mounds are smooth and featureless in appearance, offering little clues to their origin; however, they appear to occur in proximity to the channels system and are generally confined to the Amazonis Planitia geological units. Although the channels and small mounds spatially correlate, it is difficult to evaluate whether they have any geomorphological relationship. Unlike the channels, the small mounds do not appear to differ in albedo or color from the surrounding material. Similar small mounds in Utopia are not confined to the same latitude (REFS), and they occur within the Vastitas Borealis unit and do not correlate with the presence of a channel system. The Amazonis Planitia unit is believed to be volcanic/volcaniclastic in origin, whereas the Vastitas Borealis unit is believed to be fluvial, associated with large outflow channels (Tanaka et al., 2005). This suggests that the small mounds are either secondary features that formed independent of the geological unit on which they occur or that they have multiple modes of origin. Despite their differences in geological setting, both the geological units on which small mounds occur are interpreted to have undergone volatile release. Vastitas Borealis is thought to have released volatiles after being deposited as wet sediment (Kreslavsky & Head, 2002), and the Amazonis Planitia unit is thought to result from volcanic/volcaniclastic flow and subsurface ice interactions (perhaps similar to rootless cone formation, e.g., Lanagan et al., 2001). If the small mounds in Arcadia are mantled or eroded remnants of rootless cones, then they represent evidence for subsurface ice at the time that the volcanic material was deposited (i.e., Middle to Late Amazonian; Tanaka et al., 2005). The gradational boundary between the LDM, small mound and channel-dominated terrain and the platy-ridge material-dominated terrain, suggests that a lot of interesting geomorphology could be revealed in the northern plains as the LDM is removed, with landforms resulting from lava and subsurface ice interactions being uncovered.

### 5.6. Efficacy of Grid Mapping Subsurface Ice-Related Landforms in Arcadia Planitia

The mapping project required the acquisition, handling, and analysis of large numbers of high-resolution CTX images in order to identify small landforms over large areas. We elected to use the grid mapping approach to provide an efficient, consistent, and standardized approach to map the landforms indicative of subsurface ice in one examination of the data set and to promote data sharing. The speed at which the data could be recorded using the grid mapping method allowed for the first continuous, full-resolution mapping of decameter-scale landforms in CTX images on hemispherical-scale swath.

Importantly, it is a scalable approach: if a landform type needs to be split into two or more subcategories, then only those grid squares containing the parent category need to be reexamined. Hence, if in the future, more information is required for any of the landforms mapped here, a hierarchy of grids at different spatial resolutions with more detailed classifications being built up by employing smaller and smaller grids, and subclassifying individual landform types, where needed. A distinct advantage with the grid mapping approach is that it records negative results, making it possible to distinguish between the absence of landforms and absence of data. It is worth noting that carrying negative results during subclassification is only applicable if the parent category is reliably identified for all subclasses.

The method was particularly effective in mapping the distribution of the LDM by dividing the LDM into both textured and mantled subclasses. The mapping approach provided two lines of evidence that the LDM is (i) ubiquitous north of around 40°N and (ii) overlaps geological and topographical boundaries, an observation central to substantiating the hypothesis of an air fall origin. The chosen scale as 20-km by 20-km grid squares was also effective for identifying the smaller landforms such as the pitted, polygonal terrains, and small mounds. The method was less effective in mapping landforms larger than the mapping grid squares such as thumbprint terrain and large channels as they were often difficult to spot whilst *zoomed in* at CTX scale.

However, the main disadvantage of grid mapping was that it did not clarify how many specific landforms are present per mapping unit. The current method assigns the same weight to one landform as it does to a hundred. This shortcoming could be removed by recording percentage of terrain in each mapping unit occupied by each landform class, which, in turn, could clarify how much ice is present. Moreover, expanding the grid mapping to cover the whole of the northern plains would offer a much greater insight into both the distribution of landforms and their possible origins.

## 6. Conclusions

The mantled and textured signatures occur almost ubiquitously between 35°N and 78°N and have a positive spatial correlation with inferred ice stability based on thermal modeling, neutron spectroscopy, and radar data.

The degradational features into the LDM include pits, scallops, and 100-m polygons and provide supporting evidence for subsurface ice and volatile loss between 35 and 70°N in Arcadia with the mantle between 70 and 78°N appearing much more intact.

Pitted terrain appears to be much more pervasive in Arcadia than in Acidalia and Utopia suggesting that the Arcadia study area had more widespread near-surface subsurface ice and thus was more susceptible to pitting or that the ice was less well buried by sediments.

Correlations with ice stability models (Chamberlain & Boynton, 2007) suggest that lack of pits north of 65–70°N could indicate a relatively young age (~1 Ma); however, this could also be explained through regional variations in degradation rates.

Arcadia is much less scalloped than Utopia. It is possible that the scalloped terrain previously extended farther south but was removed by formation of the channel landscape. This would make the channel system very young given that the scallop formation appears to be few tens of Ma at the oldest estimates (Séjourné et al., 2011). Alternatively, the surface material in Arcadia may not be susceptible to scallop formation, whether this is due to different climatic conditions, mechanical properties, or subsurface ice content is unclear.

The ice-related landforms (namely, the LDM and its degradational forms) identified in this research are not clustered around outflow zones, tectonic features, or vents as would be expected if the ice had formed



through fluvial or groundwater outburst processes, and instead, we find the LDM to be distributed uniformly over both topographic and geological boundaries indicating that the subsurface ice in the northern plains has air fall origins.

There is an extensive channel system in Arcadia that appears to correlate with small mounds between 35 and 55°N that seems to have been partially buried by later LDM deposits. It is plausible that these channels transported large quantities of volatiles and sediments into southern Arcadia suggesting that the subsurface ice in at least southern Arcadia could contain a significant fluvial component. This is further supported by the radar reflectors for subsurface ice correlating with the area dominated by fluvial channels.

Overall, we conclude that the deposition and subsequent sublimation of the LDM are dominant in shaping the recent geomorphological landscape of northern Arcadia. The deposition of the LDM is consistent with an air fall hypothesis. However, there appears to be substantial evidence for fluvial processes in southern Arcadia. This suggests that older, underlying processes are equally dominant with the LDM and degradation thereof in shaping the landscape.

### Acknowledgments

This work is a joint effort of an International Team sponsored by the International Space Science Institute (ISSI). J. D. R. was supported by STFC (ST/L000776/1 and ST/K502212/1). M. B. was supported by grants from STFC (ST/L000776/1). V. R. E., R. J. M., L. F. T. D., and J. T. W. were supported by the Science and Technology Facilities Council (ST/P000541/1). A. L. was supported by the National Science Centre Poland (Narodowe Centrum Nauki) grant UMO-2013/08/S/ST10/00586. Data will be made available on Figshare upon acceptance for publication, temporary link: <https://figshare.com/s/279d3b383a594fe50a4d>.

### References

- Baker, V. R., Strom, R. G., Gulick, V. C., Kargel, J. S., Komatsu, G., & Kale, V. S. (1991). Ancient oceans, ice sheets, and the hydrological cycle on Mars. *Nature*, 352(6336), 589–594. <https://doi.org/10.1038/352589a0>
- Barlow, N. G., & Perez, C. N. (2003). Martian impact crater ejecta morphologies as indicators of the distribution of subsurface volatiles. *Journal of Geophysical Research*, 108(E8), 5085. <https://doi.org/10.1029/2002JE002036>
- Boynton, W. V., Feldman, W. C., Squyres, S. W., Prettyman, T. H., Brückner, J., Evans, L. G., et al. (2002). Distribution of hydrogen in the near surface of Mars: Evidence for subsurface ice deposits. *Science*, 297(5578), 81–85. <https://doi.org/10.1126/science.1073722>
- Bramson, A. M., Byrne, S., Putzig, N. E., Sutton, S., Plaut, J. J., Brothers, C., & Holt, J. W. (2015). Widespread excess ice in Arcadia Planitia, Mars. *Geophysical Research Letters*, 42, 6566–6574. <https://doi.org/10.1002/2015GL064844>
- Bridges, J. C., Seabrook, A. M., Rothery, D. A., Kim, J. R., Pillinger, C. T., Sims, M. R., et al. (2003). Selection of the landing site in Isidis Planitia of Mars probe Beagle 2. *Journal of Geophysical Research*, 108(E1), 5001. <https://doi.org/10.1029/2001JE001820>
- Bruno, B. C., Fagents, S. A., Thordarson, T., Baloga, S. M., & Pilger, E. (2004). Clustering within rootless cone groups on Iceland and Mars: Effect of nonrandom processes. *Journal of Geophysical Research*, 109, E07009. <https://doi.org/10.1029/2004JE002273>
- Buczkowski, D. L., Frey, H. V., Roark, J. H., & McGill, G. E. (2005). Buried impact craters: A topographic analysis of quasi-circular depressions, Utopia Basin, Mars. *Journal of Geophysical Research*, 110, E03007. <https://doi.org/10.1029/2004JE002324>
- Buczkowski, D. L., & Cooke, M. L. (2004). Formation of double-ring circular grabens due to volumetric compaction over buried impact craters: Implications for thickness and nature of cover material in Utopia Planitia, Mars. *Journal of Geophysical Research*, 109, E02006. <https://doi.org/10.1029/2003JE002144>
- Burr, D. M., Grier, J. A., McEwen, A. S., & Keszthelyi, L. P. (2002). Repeated aqueous flooding from the Cerberus Fossae: Evidence for very recently extant, deep groundwater on Mars. *Icarus*, 159(1), 53–73. <https://doi.org/10.1006/icar.2002.6921>
- Burr, D. M., Tanaka, K. L., & Yoshikawa, K. (2009). Pingos on Earth and Mars. *Planetary and Space Science*, 57(5–6), 541–555. <https://doi.org/10.1016/j.pss.2008.11.003>
- Byrne, S., Dundas, C. M., Kennedy, M. R., Mellon, M. T., McEwen, A. S., Cull, S. C., et al. (2009). Distribution of mid-latitude ground ice on Mars from new impact craters. *Science*, 325(5948), 1674–1676. <https://doi.org/10.1126/science.1175307>
- Cabrol, N. A., Grin, E. A., & Pollard, W. H. (2000). Possible frost mounds in an ancient Martian lake bed. *Icarus*, 145(1), 91–107. <https://doi.org/10.1006/icar.1999.6326>
- Campbell, B., Carter, L., Phillips, R., Plaut, J., Putzig, N., Safaeinili, A., et al. (2008). SHARAD radar sounding of the Vastitas Borealis Formation in Amazonis Planitia. *Journal of Geophysical Research*, 113, E12010. <https://doi.org/10.1029/2008JE003177>
- Carr, M. H., & Head, J. W. (2003). Oceans on Mars: An assessment of the observational evidence and possible fate. *Journal of Geophysical Research*, 108(E5), 5042. <https://doi.org/10.1029/2002JE001963>
- Carter, J., Poulet, F., Bibring, J.-P., & Murchie, S. (2010). Detection of hydrated silicates in crustal outcrops in the Northern Plains of Mars. *Science*, 328(5986), 1682–1686. <https://doi.org/10.1126/science.1189013>
- Chamberlain, M. A., & Boynton, W. V. (2007). Response of Martian ground ice to orbit-induced climate change. *Journal of Geophysical Research*, 112, E06009. <https://doi.org/10.1029/2006JE002801>
- Christensen, P. R., Jakosky, B. M., Kieffer, H. H., Malin, M. C., McSween, H. Y. Jr., Neelson, K., et al. (2004). The Thermal Emission Imaging System (THEMIS) for the Mars 2001 Odyssey Mission. *Space Science Reviews*, 110(1/2), 85–130. <https://doi.org/10.1023/B:SPAC.0000021008.16305.94>
- Costard, F. (1989). The spatial distribution of volatiles in the Martian hydrolithosphere. *Earth, Moon, and Planets*, 45(3), 265–290. <https://doi.org/10.1007/BF00057747>
- Costard, F., Sejourne, A., & Rygaloff, A. (2015). Evidence of recent flow activity in Acidalia Planitia, Mars. Presented at the EGU General Assembly Conference Abstracts, p. 3842.
- Costard, F. M., & Kargel, J. S. (1995). Outwash plains and thermokarst on Mars. *Icarus*, 114(1), 93–112. <https://doi.org/10.1006/icar.1995.1046>
- Costard, F., Séjourné, A., Kelfoun, K., Clifford, S., Lavigne, F., Di Pietro, I., & Bouley, S. (2017). Modeling tsunami propagation and the emplacement of thumbprint terrain in an early Mars ocean. *Journal of Geophysical Research: Planets*, 122, 633–649. <https://doi.org/10.1002/2016JE005230>
- Davis, P. A., & Tanaka, K. L. (1995). Curvilinear ridges in Isidis Planitia, Mars—The result of mud volcanism. *Lunar and Planetary Science Conference*, 26, 321–322.
- Dundas, C. M., Bramson, A. M., Ojha, L., Wray, J. J., Mellon, M. T., Byrne, S., et al. (2018). Exposed subsurface ice sheets in the Martian mid-latitudes. *Science*, 359(6372), 199–201. <https://doi.org/10.1126/science.aao1619>
- Dundas, C. M., Byrne, S., McEwen, A. S., Mellon, M. T., Kennedy, M. R., Daubar, I. J., & Saper, L. (2014). HiRISE observations of new impact craters exposing Martian ground ice. *Journal of Geophysical Research: Planets*, 119, 109–127. <https://doi.org/10.1002/2013JE004482>

- El Maarry, M. R., Markiewicz, W. J., Mellon, M. T., Goetz, W., Dohm, J. M., & Pack, A. (2010). Crater floor polygons: Desiccation patterns of ancient lakes on Mars? *Journal of Geophysical Research*, 115, E10006. <https://doi.org/10.1029/2010JE003609>
- Ewing, R. C., Peyret, A.-P. B., Kocurek, G., & Bourke, M. (2010). Dune field pattern formation and recent transporting winds in the Olympia Undae Dune Field, north polar region of Mars. *Journal of Geophysical Research*, 115, E08005. <https://doi.org/10.1029/2009JE003526>
- Feldman, W. C., Boynton, W. V., Tokar, R. L., Prettyman, T. H., Gasnault, O., Squyres, S. W., et al. (2002). Global Distribution of Neutrons from Mars: Results from Mars Odyssey. *Science*, 297(5578), 75–78. <https://doi.org/10.1126/science.1073541>
- Feldman, W. C., Prettyman, T. H., Maurice, S., Plaut, J. J., Bish, D. L., Vaniman, D. T., et al. (2004). The global distribution of near-surface hydrogen on Mars. *Journal of Geophysical Research*, 109, E09006. <https://doi.org/10.1029/2003JE002160>
- Ferguson, R. L., Christensen, P. R., & Kieffer, H. H. (2006). High-resolution thermal inertia derived from the Thermal Emission Imaging System (THEMIS): Thermal model and applications. *Journal of Geophysical Research*, 111, E12004. <https://doi.org/10.1029/2006JE002735>
- Fisher, D. A. (2005). A process to make massive ice in the Martian regolith using long-term diffusion and thermal cracking. *Icarus*, 179(2), 387–397. <https://doi.org/10.1016/j.icarus.2005.07.024>
- Forget, F., Haberle, R. M., Montmessin, F., Levrard, B., & Head, J. W. (2006). Formation of glaciers on Mars by atmospheric precipitation at high obliquity. *Science*, 311(5759), 368–371. <https://doi.org/10.1126/science.1120335>
- Frey, H. V. (2006). Impact constraints on, and a chronology for, major events in early Mars history. *Journal of Geophysical Research*, 111, E08S91. <https://doi.org/10.1029/2005JE002449>
- Gallagher, C., Balme, M., Soare, R., & Conway, S. J. (2018). Formation and degradation of chaotic terrain in the Galaxias regions of Mars: Implications for near-surface storage of ice. *Icarus*, 309, 69–83. <https://doi.org/10.1016/j.icarus.2018.03.002>
- Gallagher, C., & Balme, M. R. (2011). Landforms indicative of ground-ice thaw in the northern high latitudes of Mars. In M. R. Balme, A. S. Bargery, C. J. Gallagher, & S. Gupta (Eds.), *Martian geomorphology* (pp. 87–110). London: Geological Society of London Special Publications.
- Ghent, R. R., Anderson, S. W., & Pithawala, T. M. (2012). The formation of small cones in Isidis Planitia, Mars through mobilization of pyroclastic surge deposits. *Icarus*, 217(1), 169–183. <https://doi.org/10.1016/j.icarus.2011.10.018>
- Grizzaffi, P., & Schultz, P. H. (1989). Isidis basin: Site of ancient volatile-rich debris layer. *Icarus*, 77(2), 358–381. [https://doi.org/10.1016/0019-1035\(89\)90094-8](https://doi.org/10.1016/0019-1035(89)90094-8)
- Guidat, T., Pochat, S., Bourgeois, O., & Souček, O. (2015). Landform assemblage in Isidis Planitia, Mars: Evidence for a 3 Ga old polythermal ice sheet. *Earth and Planetary Science Letters*, 411, 253–267. <https://doi.org/10.1016/j.epsl.2014.12.002>
- Hansen, C. J., Bourke, M., Bridges, N. T., Byrne, S., Colon, C., Diniega, S., et al. (2011). Seasonal erosion and restoration of Mars' northern polar dunes. *Science*, 331(6017), 575–578. <https://doi.org/10.1126/science.1197636>
- Hiesinger, H., & Head, J. W. (2000). Characteristics and origin of polygonal terrain in southern utopia Planitia, Mars: Results from Mars Orbiter Laser Altimeter and Mars Orbiter Camera data. *Journal of Geophysical Research*, 105(E5), 11,999–12,022. <https://doi.org/10.1029/1999JE001193>
- Hartmann, W. K., Thorsteinsson, T., & Sigurdsson, F. (2003). Martian hillside gullies and Icelandic analogs. *Icarus*, 162(2), 259–277. [https://doi.org/10.1016/S0019-1035\(02\)00065-9](https://doi.org/10.1016/S0019-1035(02)00065-9)
- Head, J. W., Marchant, D. R., Dickson, J. L., Kress, A. M., & Baker, D. M. (2010). Northern mid-latitude glaciation in the Late Amazonian period of Mars: Criteria for the recognition of debris-covered glacier and valley glacier land system deposits. *Earth and Planetary Science Letters*, 294(3–4), 306–320. <https://doi.org/10.1016/j.epsl.2009.06.041>
- Head, J. W., Mustard, J. F., Kreslavsky, M., Milliken, R. E., & Marchant, D. R. (2003). Recent ice ages on Mars. *Nature*, 426(6968), 797–802. <https://doi.org/10.1038/nature02114>
- Hubbard, B., Milliken, R. E., Kargel, J. S., Limaye, A., & Souness, C. (2011). Geomorphological characterisation and interpretation of a mid-latitude glacier-like form: Hellas Planitia, Mars. *Icarus*, 211(1), 330–346. <https://doi.org/10.1016/j.icarus.2010.10.021>
- Kadish, S., Barlow, N. G., & Head, J. W. (2009). Latitude dependence of Martian pedestal craters: Evidence for a sublimation-driven formation mechanism. *Journal of Geophysical Research*, 114, E1000. <https://doi.org/10.1029/2008JE003318>
- Kargel, J. S., & Strom, R. G. (1992). Ancient glaciation on Mars. *Geology*, 20(1), 3–7. [https://doi.org/10.1130/0091-7613\(1992\)020<0003:AGOM>2.3.CO;2](https://doi.org/10.1130/0091-7613(1992)020<0003:AGOM>2.3.CO;2)
- Kargel, J. S., Strom, R. G., Lockwood, J., & Shaw, J. (1992). Subglacial and glaciomarine processes in the Martian northern plains. Presented at the Lunar and Planetary Science Conference.
- Keszthelyi, L., McEwen, A. S., & Thordarson, T. (2000). Terrestrial analogs and thermal models for Martian flood lavas. *Journal of Geophysical Research*, 105(E6), 15,027–15,049. <https://doi.org/10.1029/1999JE001191>
- Keszthelyi, L., Thordarson, T., McEwen, A., Haack, H., Guilbaud, M.-N., Self, S., & Rossi, M. J. (2004). Icelandic analogs to Martian flood lavas. *Geochemistry, Geophysics, Geosystems*, 5, Q11014. <https://doi.org/10.1029/2004GC000758>
- Kostama, V.-P., Kreslavsky, M. A., & Head, J. W. (2006). Recent high-latitude icy mantle in the northern plains of Mars: Characteristics and ages of emplacement. *Geophysical Research Letters*, 33, L11201. <https://doi.org/10.1029/2006GL025946>
- Kreslavsky, M. A., & Head, J. W. (2002). Mars: Nature and evolution of young latitude-dependent water-ice-rich mantle. *Journal of Geophysical Research*, 29(15), 1719. <https://doi.org/10.1029/2002GL015392>
- Lanagan, P. D., McEwen, A. S., Keszthelyi, L. P., & Thordarson, T. (2001). Rootless cones on Mars indicating the presence of shallow equatorial ground ice in recent times. *Geophysical Research Letters*, 28(12), 2365–2367. <https://doi.org/10.1029/2001GL012932>
- Lane, M. D., & Christensen, P. R. (2000). Convection in a catastrophic flood deposit as the mechanism for the giant polygons on Mars. *Journal of Geophysical Research*, 105(E7), 17,617–17,627. <https://doi.org/10.1029/1999JE001197>
- Laskar, J., Correia, A. C. M., Gastineau, M., Joutel, F., Levrard, B., & Robutel, P. (2004). Long term evolution and chaotic diffusion of the insolation quantities of Mars. *Icarus*, 170(2), 343–364. <https://doi.org/10.1016/j.icarus.2004.04.005>
- Levy, J., Head, J., & Marchant, D. (2009). Thermal contraction crack polygons on Mars: Classification, distribution, and climate implications from HiRISE observations. *Journal of Geophysical Research*, 114, E01007. <https://doi.org/10.1029/2008JE003273>
- Levy, J. S., Marchant, D. R., & Head, J. W. (2010). Thermal contraction crack polygons on Mars: A synthesis from HiRISE, Phoenix, and terrestrial analog studies. *Icarus*, 206(1), 229–252. <https://doi.org/10.1016/j.icarus.2009.09.005>
- Lockwood, J. F., Kargel, J. S., & Strom, R. B. (1992). Thumbprint terrain on the northern plains: A glacial hypothesis. Presented at the Lunar and Planetary Science Conference, p. 795.
- Lucchitta, B. K., Ferguson, H. M., & Summers, C. (1986). Sedimentary deposits in the Northern Lowland Plains, Mars. *Journal of Geophysical Research*, 91(B13), E166–E174. <https://doi.org/10.1029/JB091iB13p0E166>
- Mahaney, W. C., Milner, M. W., Netoff, D. I., Malloch, D., Dohm, J. M., Baker, V. R., et al. (2004). Ancient wet aeolian environments on Earth: Clues to presence of fossil/live microorganisms on Mars. *Icarus*, 171(1), 39–53. <https://doi.org/10.1016/j.icarus.2004.04.014>

- Malin, M. C., Bell, J. F., Cantor, B. A., Caplinger, M. A., Calvin, W. M., Clancy, R. T., et al. (2007). Context Camera investigation on board the Mars Reconnaissance Orbiter. *Journal of Geophysical Research*, 112, E05S04. <https://doi.org/10.1029/2006JE002808>
- Malin, M. C., & Edgett, K. S. (2000). Evidence for recent groundwater seepage and surface runoff on Mars. *Science*, 288(5475), 2330–2335. <https://doi.org/10.1126/science.288.5475.2330>
- Mangold, N. (2005). High latitude patterned ground on Mars: Classification, distribution and climatic control. *Icarus*, 174(2), 336–359. <https://doi.org/10.1016/j.icarus.2004.07.030>
- McGill, G. E. (1986). The giant polygons of Utopia, northern Martian Plains. *Geophysical Research Letters*, 13(8), 705–708. <https://doi.org/10.1029/GL013i008p00705>
- McGill, G. E., & Hills, L. S. (1992). Origin of giant Martian polygons. *Journal of Geophysical Research*, 97(E2), 2633–2647. <https://doi.org/10.1029/91JE02863>
- Mellon, M. T., Arvidson, R. E., Sizemore, H. G., Searls, M. L., Blaney, D. L., Cull, S., et al. (2009). Ground ice at the Phoenix landing site: Stability state and origin. *Journal of Geophysical Research*, 114, E00E07. <https://doi.org/10.1029/2009JE003417>
- Milliken, R. E., Mustard, J. F., & Goldsby, D. L. (2003). Viscous flow features on the surface of Mars: Observations from high-resolution Mars Orbiter Camera (MOC) images. *Journal of Geophysical Research*, 108(E6), 5057. <https://doi.org/10.1029/2002JE002005>
- Morgenstern, A., Hauber, E., Reiss, D., van Gasselt, S., Grosse, G., & Schirrmeyer, L. (2007). Deposition and degradation of a volatile-rich layer in Utopia Planitia and implications for climate history on Mars. *Journal of Geophysical Research*, 112, E06010. <https://doi.org/10.1029/2006JE002869>
- Mouginot, J., Pommerol, A., Beck, P., Kofman, W., & Clifford, S. M. (2012). Dielectric map of the Martian northern hemisphere and the nature of plain filling materials. *Geophysical Research Letters*, 39, L02202. <https://doi.org/10.1029/2011GL050286>
- Mustard, J. F., Cooper, C. D., & Rifkin, M. K. (2001). Evidence for recent climate change on Mars from the identification of youthful near-surface ground ice. *Nature*, 412(6845), 411–414. <https://doi.org/10.1038/35086515>
- Orgel, C., Hauber, E., van Gasselt, S., Pozzobon, R., & Skinner, J., Jr. (2016). Distribution, origin and evolution of hypothesized mud volcanoes, thumbprint terrain, small mounds and giant polygons: Implications for sedimentary processes in the northern lowlands of Mars: Case study from the Acidalia Planitia. Presented at the EGU General Assembly Conference Abstracts, p. 1038.
- Orgel, C., Hauber, E., van Gasselt, S., Reiss, D., Johnsson, A., Ramsdale, J. D., et al. (2018). Grid mapping the northern plains of Mars: A new overview of recent water- and ice-related landforms in Acidalia Planitia. *Journal of Geophysical Research: Planets*, 123. <https://doi.org/10.1029/2018JE005664>
- Page, D. P., Balme, M. R., & Grady, M. M. (2009). Dating martian climate change. *Icarus*, 203(2), 376–389. <https://doi.org/10.1016/j.icarus.2009.05.012>
- Pechmann, J. C. (1980). The origin of polygonal troughs on the Northern Plains of Mars. *Icarus*, 42(2), 185–210. [https://doi.org/10.1016/0019-1035\(80\)90071-8](https://doi.org/10.1016/0019-1035(80)90071-8)
- Plescia, J. B. (1980). Cinder cones of Isidis and Elysium. *Reports of Planetary Geology Program*, 1, 263–265.
- Plescia, J. B. (1990). Recent flood lavas in the Elysium region of Mars. *Icarus*, 88(2), 465–490. [https://doi.org/10.1016/0019-1035\(90\)90095-Q](https://doi.org/10.1016/0019-1035(90)90095-Q)
- Plescia, J. B. (2003). Cerberus Fossae, Elysium, Mars: A source for lava and water. *Icarus*, 164(1), 79–95. [https://doi.org/10.1016/S0019-1035\(03\)00139-8](https://doi.org/10.1016/S0019-1035(03)00139-8)
- Ramsdale, J. D., Balme, M. R., Conway, S. J., Gallagher, C., van Gasselt, S. A., Hauber, E., et al. (2017). Grid-based mapping: A method for rapidly determining the spatial distributions of small features over very large areas. *Planetary and Space Science*, 140, 49–61. <https://doi.org/10.1016/j.pss.2017.04.002>
- Roszbacher, L. A., & Judson, S. (1981). Ground ice on Mars: Inventory, distribution, and resulting landforms. *Icarus*, 45(1), 39–59. [https://doi.org/10.1016/0019-1035\(81\)90005-1](https://doi.org/10.1016/0019-1035(81)90005-1)
- Schaefer, M. W. (1990). Karst on Mars? The thumbprint terrain. *Icarus*, 83(1), 244–247. [https://doi.org/10.1016/0019-1035\(90\)90017-4](https://doi.org/10.1016/0019-1035(90)90017-4)
- Schon, S. C., Head, J. W., & Fassett, C. I. (2012). Recent high-latitude resurfacing by a climate-related latitude-dependent mantle: Constraining age of emplacement from counts of small craters. *Planetary and Space Science*, 69(1), 49–61. <https://doi.org/10.1016/j.pss.2012.03.015>
- Scott, D. H., & Underwood, J. R., Jr. (1991). Mottled terrain—A continuing Martian enigma. Presented at the Lunar and Planetary Science Conference Proceedings, pp. 627–634.
- Séjourné, A., Costard, F., Gargani, J., Soare, R. J., Fedorov, A., & Marmo, C. (2011). Scalloped depressions and small-sized polygons in western Utopia Planitia, Mars: A new formation hypothesis. *Planetary and Space Science*, 59(5-6), 412–422. <https://doi.org/10.1016/j.pss.2011.01.007>
- Séjourné, A., Costard, F., Gargani, J., Soare, R. J., & Marmo, C. (2012). Evidence of an eolian ice-rich and stratified permafrost in Utopia Planitia, Mars. *Planetary and Space Science*, 60(1), 248–254. <https://doi.org/10.1016/j.pss.2011.09.004>
- Séjourné, A., Costard, F., Swirad, Z. M., Łosiak, A., Bouley, S., Smith, I., et al. (2018). Grid mapping the northern plains of Mars: Using morphotype and distribution of ice-related landforms to understand multiple ice-rich deposits in Utopia Planitia. *Journal of Geophysical Research: Planets*, 123. <https://doi.org/10.1029/2018JE005665>
- Sizemore, H. G., Zent, A. P., & Rempel, A. W. (2015). Initiation and growth of Martian ice lenses. *Icarus, Dynamic Mars*, 251, 191–210. <https://doi.org/10.1016/j.icarus.2014.04.013>
- Skinner, J. A., Tanaka, K. L., & Platz, T. (2012). Widespread loess-like deposit in the Martian northern lowlands identifies Middle Amazonian climate change. *Geology*, 40(12), 1127–1130. <https://doi.org/10.1130/G33513.1>
- Smith, D. E., Zuber, M. T., Frey, H. V., Garvin, J. B., Head, J. W., Muhleman, D. O., et al. (2001). Mars Orbiter Laser Altimeter: Experiment summary after the first year of global mapping of Mars. *Journal of Geophysical Research*, 106(E10), 23,689–23,722. <https://doi.org/10.1029/2000JE001364>
- Smith, I. B., & Holt, J. W. (2015). Spiral trough diversity on the north pole of Mars, as seen by Shallow Radar (SHARAD). *Journal of Geophysical Research: Planets*, 120, 362–387. <https://doi.org/10.1002/2014JE004720>
- Soare, R. J., Burr, D. M., & Wan Bun Tseung, J.-M. (2005). Possible pingos and a periglacial landscape in northwest Utopia Planitia. *Icarus*, 174(2), 373–382. <https://doi.org/10.1016/j.icarus.2004.11.013>
- Soare, R. J., Conway, S. J., & Dohm, J. M. (2014). Possible ice-wedge polygons and recent landscape modification by “wet” periglacial processes in and around the Argyre impact basin, Mars. *Icarus*, 233, 214–228. <https://doi.org/10.1016/j.icarus.2014.01.034>
- Soare, R. J., Conway, S. J., Gallagher, C., & Dohm, J. M. (2017). Ice-rich (periglacial) vs icy (glacial) depressions in the Argyre region, Mars: A proposed cold-climate dichotomy of landforms. *Icarus*, 282, 70–83. <https://doi.org/10.1016/j.icarus.2016.09.009>
- Soare, R. J., Kargel, J. S., Osinski, G. R., & Costard, F. (2007). Thermokarst processes and the origin of crater-rim gullies in Utopia and western Elysium Planitia. *Icarus*, 191(1), 95–112. <https://doi.org/10.1016/j.icarus.2007.04.018>
- Souness, C., & Hubbard, B. (2012). Mid-latitude glaciation on Mars. *Progress in Physical Geography*, 36(2), 238–261. <https://doi.org/10.1177/0309133312436570>

- Souness, C., Hubbard, B., Milliken, R. E., & Quincey, D. (2012). An inventory and population-scale analysis of Martian glacier-like forms. *Icarus*, 217(1), 243–255. <https://doi.org/10.1016/j.icarus.2011.10.020>
- Squyres, S. W., & Carr, M. H. (1986). Geomorphic evidence for the distribution of ground ice on Mars. *Science*, 231(4735), 249–252. <https://doi.org/10.1126/science.231.4735.249>
- Tanaka, K. L., & Kolb, E. J. (2001). Geologic history of the polar regions of Mars based on Mars Global Surveyor Data: I. Noachian and Hesperian periods. *Icarus*, 154(1), 3–21. <https://doi.org/10.1006/icar.2001.6675>
- Tanaka, K. L., Skinner, J. A., Dohm, J. M., Irwin, R. P., Fortezzo, C. M., & Platz, T., et al. (2014). Geologic map of Mars SIM 3292. U.S. Geological Survey Scientific Investigations.
- Tanaka, K. L., Skinner, J. A., & Hare, T. M. (2005). Geologic map of the northern plains of Mars. U.S. Geol. Surv. Misc. invest. Ser. Map I-2888.
- Taylor Perron, J., Mitrovica, J. X., Manga, M., Matsuyama, I., & Richards, M. A. (2007). Evidence for an ancient Martian ocean in the topography of deformed shorelines. *Nature*, 447(7146), 840–843. <https://doi.org/10.1038/nature05873>
- Ulrich, M., Hauber, E., Herzsuh, U., Härtel, S., & Schirrmeister, L. (2011). Polygon pattern geomorphometry on Svalbard (Norway) and western Utopia Planitia (Mars) using high-resolution stereo remote-sensing data. *Geomorphology*, 134(3–4), 197–216. <https://doi.org/10.1016/j.geomorph.2011.07.002>
- Ulrich, M., Morgenstern, A., Günther, F., Reiss, D., Bauch, K. E., Hauber, E., et al. (2010). Thermokarst in Siberian ice-rich permafrost: Comparison to asymmetric scalloped depressions on Mars. *Journal of Geophysical Research*, 115, E10009. <https://doi.org/10.1029/2010JE003640>
- Viola, D., McEwen, A. S., Dundas, C. M., & Byrne, S. (2015). Expanded secondary craters in the Arcadia Planitia region, Mars: Evidence for tens of Myr-old shallow subsurface ice. *Icarus*, 248, 190–204. <https://doi.org/10.1016/j.icarus.2014.10.032>
- Wilson, J. T., Eke, V. R., Massey, R. J., Elphic, R. C., Feldman, W. C., Maurice, S., & Teodoro, L. F. A. (2018). Equatorial locations of water on Mars: Improved resolution maps based on Mars Odyssey Neutron Spectrometer data. *Icarus*, 299, 148–160. <https://doi.org/10.1016/j.icarus.2017.07.028>